國立台灣大學理學院物理學系
碩士論文
Department of Physics
College of Science
National Taiwan University
Master Thesis

單量子點之光輔助穿遂現象的記憶效應：以廣義Floquet理論分析

Memory effect on the photon-assisted tunneling through a single quantum dot: Generalized Floquet approach

陳信達
Hsing-Ta Chen

指導教授：朱時宜 博士
Advisor: Shih-I Chu, Ph.D.

中華民國99年7月
July, 2010

國立臺灣大學碩士學位論文
口試委員會審定書

單量子點之光輔助穿遂現象的記憶效應：
以廣義 Floquet 理論分析

Memory effect on the photon-assisted tunneling through a single quantum dot: Generalized Floquet approach

本論文係陳信達君（R96222072）在國立臺灣大學物理學研究所完成之碩士學位論文，於民國 99 年 7 月 1 日承下列考試委員審查通過及口試及格，特此證明

口試委員：朱時宜（簽名）

（指導教授）

鄭厚忠　　管希聖

_____　　_____

_____　　_____

Contents

List of Figures

Abstract

The generalized Floquet approach is extended to sutdy the memory effect beyond the wide band limit on the photon-assisted electron tunneling through a periodically driven single quantum dot. An analytical Tien-Gordon-like expression, including the memory effect, for the current and transmission coefficient is derived based on the generalized Van Vleck (GVV) nearly degenerate perturbation theory. As a result, multiphoton (MP) coherent destruction of tunneling (CDT) phenomenon for small bias voltage is predicted by the transmission coefficients for the respective scattering channels. Numerically converged simulations and GVV analytical results are compared and both reveal that the memory effect leads to the suppression of the d.c. current stair-step jumps when varying the bias voltage on the single quantum dot. Furthermore, a novel blockade phenomenon that does not exist in the wide band limit is observed when the memory effect becomes significant, showing that the pumped current oscillate distinctively with respect to the gate voltage in the in the large bias limit. Finally, analytical expressions are obtained in the wide band limit, showing the temperature dependence of the conductance and current.

摘　要

本文利用廣義Floquet理論研究單一量子點的傳輸行為，尤其著重於光子輔助穿遂現象的記憶效應。藉由廣義Floquet理論，我們可以將一具週期性的薛丁格方程，改寫成一個與時間無關且無限維度的等效方程。利用微擾分析得到解析結果，進而推導出包含記憶效應之電流與穿遂係數表示式。在此架構下，我們探討記憶效應對光子輔助穿遂現象的影響，其中包含多光子同調穿隧截止現象、電流梯級現象、庫倫阻塞現象。另外，我們探討溫度對於電子傳輸的影響。

謝　辭

首先要感謝我的指導教授朱時宜老師。一如我們初次見面，朱老師對物理學的熱情依然能夠讓我滿腔熱血地離開老師的辦公室。老師的悉心指導領著我一窺這個嶄新蓬勃的研究領域，也激發我對投入研究工作的興趣。

我也要感謝遠在美國的何德生老師。在研究的道路上，老師給予我無可取代的支持與討論，老師對於科學研究嚴謹且謙虛的態度，也深深影響我對學術研究的看法。另外，化學系鄭原忠老師不僅僅在研究工作上給與批評與指點，也是我在感到困惑時，最好的討論對象。

感謝實驗室的夥伴們，一起工作討論的洪士涵，聊天聊地練英文還可以問問題的阿強和老黃。感謝總是互相砥礪的鄭富元、張中懷、陳佑航、廖馬克、小剛、賴盈樺、劉怡麟、陳怡臻。沒有你們的陪伴，實驗室的氣氛不會如此融洽。

女友岱萱總是在背後默默的支持，忍受我在這過程中所有的不安與焦慮，以及因為我專心於研究而造成的忽略。

最後，本論文獻給期待卻無緣見到這一切的母親，感謝你始終相信我做的決定，並永遠作為我進步的原動力。

Chapter 1

Introduction

1.1 Photon-assisted Tunneling

Electron transport of a quantum system in the presence of time-dependent external fields has been studied by various approaches, often leading to observation of new phenomena and applications. The early experiment conducted by Dayem and Martin in 1962 [1] studied the photon-assisted tunneling (PAT) processes in hybrid structures with an insulator film sandwiched by two superconductors as source and drain. The time-periodic fields (the microwave field) were applied to the source and drain. Soon after, Tien and Gordon (TG) proposed a simple theoretical model of the PAT in 1963 [2], suggesting that a time-dependent periodic external field, of the amplitude A and frequency ω, can induce distinctive sideband structures of the electron density in the source and drain. Each sideband accounts for a multi-photon inelastic scattering process off an electron with the incident energy E. A sideband involving m photons can be effectively viewed as forming an electron density of state at the energy $E + m\hbar\omega$ for the absorption processes (or $E - m\hbar\omega$

for the emission processes), with the density equal to the squared of the mth order Bessel function of the first kind $J_m^2(A/\hbar\omega)$. The resultant d.c. current $\bar{I}$ in the presence of the external field can then be expressed as $\bar{I} = \sum J_m^2(A/\hbar\omega) \times I_m$ in terms of the field-free partial currents I_m in the absence of the external field.

In the past two decades, due to the advent of the nanotechnology, the effect of time-dependent fields on the coherent tunneling through a single quantum dot (SQD) has been widely investigated experimentally and theoretically. On the experimental side, the PAT has been studied in various nanoscale system, including GaAs/AlGaAs quantum dots [3, 4, 5, 6], single-donor quantum dots in semiconductor nanostructure [7, 8], and carbon nanotube quantum dots [9]. Especially, the Coulomb blockade phenomena, such as the stair-step d.c. current and the pumped current oscillation, around zero bias voltage have been observed. On the theoretical side, various models of nanoscale PAT have been formulated based on, for example, the quantum master equation approaches [10, 11] and the scattering theory in the context of the non-equilibrium Green's function (NEGF) method [12, 13, 14, 15]. The PAT absorption/emission sideband structures revealed in these studies agreed with the experimental findings. Novel phenomena and properties of PAT have been widely discussed, including the temperature dependence of the conductance [16, 17], multiple photon assisted tunneling phenomena [18, 19], the excess noise [20] , and the band structure effects [21]. Recently, there have been studies focussing on the nanoscale system with the external driving field applied only on the SQD tunneling device [22]. It provided a feasible method to implement quantum coherent control by applying a laser field. Shot-noise control [23] and current suppression by coherent destruction of tunneling (CDT) [24, 25, 26, 27, 28]. It is noteworthy that, in most of previous works, electron transport are usually studied within the wide band limit: the spectral density of electrode

is assumed energy-independent.

Beyond the wide band limit, memory effect (the effect of energy-dependent spectral density) can be addressed by mimicking the spectral density as a collection of Lorentzian functions [29, 30, 31, 32]. Recently, a generalized Floquet approach adopting the Lorentzian spectral density (LSD) is developed for the general treatment of memory effect on driven quantum transport systems [32]. Mathematically, LSD can convert the integro-differential equations with memory kernel into a set of coupled ordinary differential equations that can be efficiently treated by the generalized Floquet approach. In addition, an effective model with generalized Hamiltonian (non-Hermittian) can be obtained to illustrate physical insights.

1.2 Generalized Floquet formalisms

In 1965, the Floquet matrix method was first proposed by J.H. Shirley in [33], for the nonperturbative treatment for the multi-photon transitions in two-level systems in periodic fields. However, the conventional Floquet theorem [34], requiring the Hamiltonian to be periodic in time, and the Floquet matrix method [33] can only be applied to the bound-bound transitions of a few level systems in monochromatic fields and cannot be used to treat the bound-free and free-free transitions of realistic atomic and molecular systems in intense laser fields.

In the last few decades, a number of generalized Floquet formalisms have been developed to go beyond the conventional Floquet theorem [34]. Given below is a brief survey of some of these generalized Floquet theoretical developments. For the reviews of these new developments, we refer to references [35, 36, 37].

In 1979, Chu and Reinhardt extended the complex scaling transformation and developed the non-Hermitian Floquet formalism and complex quasi-energy method for the first nonperturbative treatment of multiphoton ionization (MPI) and bound-free transitions of infinite-level atomic systems [38]. The non-Hermitian Floquet formalism was later further extended to the treatment of MPI and above-threshold ionization (ATI) of atomic systems [39, 40, 41], and multiphoton dissociation (MPD) and above-threshold dissociation (ATD) of molecular systems [42, 43, 44, 45] and a number of other highly nonlinear atomic and molecular multiphoton processes such as high-order harmonic generation (HHG), etc. [35, 36, 37].

The conventional Floquet theorem and Floquet matrix methods cannot be used to treat dynamical processes with non-periodic time-dependent Hamiltonian. Such a bottleneck was overcome In 1983, when the many-mode Floquet theorem (MMFT) was developed by Ho, Tietz, and Chu [46], allowing the exact treatment of multiphoton processes in non-periodic external fields, such as polychromatic or quasi-periodic time-dependent fields. The MMFT allows the exact transformation of the time-dependent Schrödinger equation into a time-independent many-mode Floquet Hamiltonian, providing powerful nonperturbative approach for the treatment of multiphoton bound-bound [47, 48], and bound-free transitions, such as MPI/ATI/ATD [49] and HHG [50] processes in intense two-color or polychromatic laser fields with incommensurate frequencies.

Another major advancement of the generalized Floquet formalism is the development of the Floquet-Liouville supermatrix (FLSM) formalism by Ho, Wang, and Chu in 1985 [51, 52, 53]. The FLSM formalism provides a nonperturbative approach for the accurate treatment of the time-dependent Liouville equation with non-periodical time-dependent Hamiltonian with energy relaxation and decoherence. The FLSM approach allows the

exact transformation of the time-dependent Liouville equation into an equivalent time-independent infinite-dimensional super-eigenvalue equation. The approach has been applied to the study of resonance fluorescence [52] and nonlinear optical susceptibilities [53] in intense polychromatic laser fields with insightful new predictions of various nonlinear optical phenomena. Recent extension of the FLSM has been made to the study of time-resolved measurement of dissipation-induced decoherence in a Josephson junction [54] and coherent temporal oscillations of macroscopic quantum states in a Josephson junction [55], etc.

We note that for the treatment of bound-bound near-resonant multiphoton transitions within the generalized Floquet matrix approach, the generalized Van Vleck (GVV) nearly degenerate perturbation method [56, 57] can be adopted, allowing the reduction of the infinite-dimensional Floquet matrix of N-level systems, into an $N \times N$ effective Hamiltonian, from which insightful analytical expressions for the transition probability, etc., can be obtained. The GVV approach is well beyond the conventional rotating wave approximation (RWA) and takes into account the level shift and power broadening effects. In this thesis, we'll adopt the generalized Floquet approach and the GVV method for the study of electron quantum transport.

1.3 structure of the thesis

The thesis is organized as follows. In the chapter 2, first, we describe the general formulation of the single quantum dot system and the scattering formalism. All the necessary tools are introduced, including the Lorentzian spectral density and the generalized Floquet formulation. In chapter 3, we implement the generalized Floquet formulation and calculate

the transmission coefficient and the d.c. current to represent the coherent destruction of tunneling and blockade phenomena. In chapter 4, we consider the symmetric Lorentzian spectral density and derive the Tien-Gordon-like formula by the generalized Van Vleck (GVV) nearly-degenerate perturbation method. The analytical GVV result are compared with the numerical one. compare the GVV analytical result and exact Floquet calculation, and discuss the interplay of the bias voltage and the LSD band width. In chapter 5, the temperature-dependence of the current and the conductance are discussed within the wide band limit. Finally, a conclusion is given in the chapter 6.

Chapter 2

General Formulation

2.1 The tight-binding model and scattering formalism

We consider a single quantum dot (SQD) in contact with a left electrode (source) and a right electrode (drain), as shown in Fig. 2.1. The SQD possesses a single energy level and is driven by an external time-dependent field $A(t)$. In the tight-binding (TB) model, the corresponding electrode-SQD-electrode Hamiltonian can be written as [22, 23],

$$H(t) = H_C(t) + \sum_{\ell=L,R} H_\ell + H'. \tag{2.1}$$

Here $H_C(t) = [\epsilon_0 + A(t)]|0\rangle\langle 0|$ is the periodically driven SQD Hamiltonian, in which ϵ_0 is the on-site energy associated with the state $|0\rangle$ driven by a periodic external field $A(t)$, $A(t+T) = A(t)$; $H_\ell = \sum_q \epsilon_{\ell q}|\ell q\rangle\langle \ell q|$, $\ell = L, R$, are, respectively, the left and right electrode Hamiltonians defined by the electron states $|\ell q\rangle$ having the on-site energy $\epsilon_{\ell q}$;

and

$$H' = \sum_{Lq} V_{Lq}|Lq\rangle\langle 0| + \sum_{Rq} V_{Rq}|Rq\rangle\langle 0| + h.c. \tag{2.2}$$

represents the contact Hamiltonian between the SQD and two electrodes via the corresponding coupling parameters V_{Lq} and V_{Rq}, respectively.

Within the framework of the non-equilibrium Green's functions (NEGF) method [13], the corresponding single-particle retarded Green's function can be computed via the relation

$$G(t,\epsilon) = G(t+T,\epsilon) = \frac{1}{\imath\hbar}\int_0^\infty \mathrm{e}^{\imath\epsilon t'/\hbar} U(t,t-t')dt',\ t \geq t' \geq 0, \tag{2.3}$$

where $U(t+T,t_0+T) = U(t,t_0)$ is the underlying single particle propagator for the periodically driven electrode-SQD-electrode system. The kth-order Fourier coefficient

$$G^{(k)}(\epsilon) = \frac{1}{T}\int_0^T G(t,\epsilon)\mathrm{e}^{\imath k\omega t}dt, \tag{2.4}$$

of the retarded Green's function $G(t,\epsilon)$ denotes the single particle, with an incident energy ϵ, undergoing absorption or emission of $|k|$ photons [22]. The transmission coefficient of the electron tunneling in the k-photon process is [23]

$$T^{(k)}_{LR/RL}(\epsilon) = \frac{1}{4}\bar{\Gamma}_{L/R}(\epsilon + k\hbar\omega)\bar{\Gamma}_{R/L}(\epsilon)|G^{(k)}(\epsilon)|^2, \tag{2.5}$$

which in turn leads to the total transmission coefficient of electron through SQD:

$$T_{LR/RL}(\epsilon) = \frac{1}{4}\sum_{k=-\infty}^{\infty} \bar{\Gamma}_{L/R}(\epsilon + k\hbar\omega)\bar{\Gamma}_{R/L}(\epsilon)|G^{(k)}(\epsilon)|^2, \tag{2.6}$$

where the spectral density of coupled electron, $\Gamma_{R/L}(\epsilon)$, are related to the coupling param-

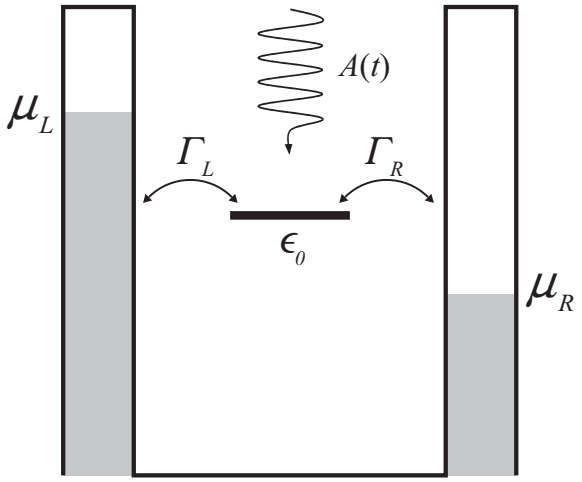

Figure 2.1: Energy diagram of the SQD that possesses a single energy level ϵ_0 and is driven by an external field $A(t)$. The Fermi energy of two electrodes are denoted as μ_L and μ_R respectively. The coupling between the SQD and the electrodes are represented by the spectral density $\bar{\Gamma}_L(\epsilon)$ and $\bar{\Gamma}_R(\epsilon)$.

eters and will be discussed in the next section. Thus, the time-ensemble averaged current (the d.c. current) can be expressed in terms of the total transmission coefficients:

$$\bar{I} = \frac{e}{h}\int_{-\infty}^{\infty} \{T_{LR}(\epsilon) f_R(\epsilon) - T_{RL}(\epsilon) f_L(\epsilon)\}\, d\epsilon, \tag{2.7}$$

where $f_\ell(\epsilon) = 1/\{1 + \mathrm{e}^{(\epsilon-\mu_\ell)/k_B\mathcal{T}}\}$ is the the Fermi-Dirac function at temperature $\mathcal{T}$, with μ_ℓ being the corresponding electrochemical potential. The difference $\mu_R - \mu_L$ is the bias voltage across the SQD. In the zero temperature limit, i.e. $\mathcal{T} = 0$, the Fermi-Dirac function reduces to a step function bounded by the bias voltage window $[\mu_L, \mu_R]$.

The initial densities are given as, $\rho = \mathrm{e}^{-(H_L+H_R-\mu_L N_L \mu_R N_R)/k_B\mathcal{T}}$, where N_L and N_R are the number operators of the left and right electrodes. We focus on the long-term behavior by consider the limit $t_0 \to -\infty$, which eliminating all the transient contributions. Thus, with this limit condition, we can project the Heisenburg equation of motion for entire system onto a integro-differential equation for the single particle propagator of the central part [23]. In terms of the coupling parameters, V_{Lq} and V_{Rq}, the underlying SQD

single-particle propagator $U(t,t_0)$ satisfies the time-dependent integro-differential equation:

$$\imath\hbar\frac{d}{dt}U(t,t_0) = H_C(t)U(t,t_0) - \frac{\imath}{\hbar}\int_{t_0}^{t}\sum_{\ell,q}|V_{\ell q}|^2\mathrm{e}^{-\epsilon_{\ell q}(t-t')/\hbar}U(t',t_0)dt'. \tag{2.8}$$

In order to match up with the conventional wide band limit, we define the response function (memory kernel) as

$$\bar{\Gamma}_\ell(t-t') = \frac{2}{\hbar}\sum_q |V_{\ell q}|^2\mathrm{e}^{-\imath\epsilon_{\ell q}(t-t')/\hbar}, \tag{2.9}$$

representing the memory effect of the electrodes on the SQD.The Fourier transformation of the response function (the spectral density), $\bar{\Gamma}_\ell(\epsilon) = \int\bar{\Gamma}_\ell(t)\mathrm{e}^{\imath\epsilon t/\hbar}dt$, can in principle be written as a collection of delta functions at individual energy levels weighted by the corresponding coupling parameters,

$$\bar{\Gamma}_\ell(\epsilon) = 4\pi\sum_q |V_{\ell q}|^2\delta(\epsilon-\epsilon_q). \tag{2.10}$$

2.2 Lorentzian spectral density model and effective Schrödinger equation

In practice, we model the spectral density $\bar{\Gamma}_\ell(\epsilon)$ by a sum of M Lorentzian functions, i.e., an M functions Lorentzian spectral density (LSD) model [32]

$$\bar{\Gamma}_\ell(\epsilon) = \sum_{k=1}^{M}\frac{a_k^\ell b_k^\ell}{(\epsilon-\sigma_k^\ell)^2+(b_k^\ell)^2}, \tag{2.11}$$

where a_k^ℓ, b_k^ℓ and σ_k^ℓ are the LSD fitting parameters. Here $\Gamma_k^\ell (\equiv a_k^\ell / b_k^\ell)$, b_k^ℓ and σ_k^ℓ denote the coupling strength, the band-width and the peak position, respectively, of the kth Lorentzian function. By the inverse relation, $\bar{\Gamma}_\ell(t) = \frac{1}{2\pi\hbar}\int \bar{\Gamma}_\ell(\epsilon) \mathrm{e}^{-\imath\epsilon t/\hbar} d\epsilon$, the LSD response function can be expressed as

$$\begin{aligned} \bar{\Gamma}_\ell(t-t') &= \frac{1}{2\pi\hbar}\sum_{k=1}^{M}\int \frac{a_k^\ell b_k^\ell}{(\epsilon-\sigma_k^\ell)^2+(b_k^\ell)^2}\mathrm{e}^{-\imath\epsilon(t-t')/\hbar}d\epsilon \\ &= \frac{1}{2\hbar}\sum_{k=1}^{M} a_k^\ell \mathrm{e}^{-\imath(\sigma_k^\ell - \imath b_k^\ell)(t-t')/\hbar}. \end{aligned} \tag{2.12}$$

In the wide band limit (WBL), we have $b_k^\ell \to \infty$, thus $\sum_k \Gamma_k^\ell \to \Gamma_\ell$. In the WBL, the spectral density $\bar{\Gamma}_\ell(\epsilon)$ is independent of the energy, i.e., $\bar{\Gamma}_\ell(\epsilon) \to \Gamma_\ell$. Consequently, the WBL response function is a delta function, i.e., $\bar{\Gamma}_\ell(t-t') = \Gamma_\ell \times \delta(t-t')$, which contains no memory effect,

$$\imath\hbar\frac{d}{dt}U(t,t_0) = H_C(t)U(t,t_0) - \frac{\imath}{2}\sum_{\ell=L,R}\Gamma_\ell U(t,t_0), \tag{2.13}$$

that will be discussed in chapter 2.

Therefore, in terms of the memory kernel, we express the integro-differential equation:

$$\imath\hbar\frac{d}{dt}U(t,t_0) = H_C(t)U(t,t_0) - \frac{\imath}{2}\int_{t_0}^{t}\sum_{\ell=L,R}\bar{\Gamma}_\ell(t-t')U(t',t_0)dt', \tag{2.14}$$

In chapter 4 and 5, we focus on the memory effect on the d.c. current through SQD using a single function LSD model, i.e. $M = 1$ in Eq. (2.11), with a peak position σ^ℓ and finite

band width $b^\ell < \infty$. By invoking Eq. (2.12) and introducing the auxiliary functions

$$Y^\ell(t,t_0) = -\frac{1}{2\hbar}\int_{t_0}^{t} \sqrt{a^\ell}\exp[-\imath(\sigma^\ell - \imath b^\ell)(t-t')/\hbar] \times U(t',t_0)dt',\ \ell = L,R, \quad (2.15)$$

Eq. (2.14) can be cast as a set of coupled ordinary differential equations of three complex scalar functions $U(t,t_0)$, $Y^L(t,t_0)$ and $Y^R(t,t_0)$, i. e.,

$$\imath\hbar\frac{d}{dt}\begin{pmatrix} U(t,t_0) \\ Y^L(t,t_0) \\ Y^R(t,t_0) \end{pmatrix} = \mathcal{H}(t)\begin{pmatrix} U(t,t_0) \\ Y^L(t,t_0) \\ Y^R(t,t_0) \end{pmatrix}, \quad (2.16)$$

subject to the initial conditions $U(t_0,t_0) = 1$, $Y^L(t_0,t_0) = 0$, and $Y^R(t_0,t_0) = 0$, where

$$\mathcal{H}(t) = \begin{pmatrix} \epsilon_0 + A(t) & \imath\sqrt{a^L}/2 & \imath\sqrt{a^R}/2 \\ -\imath\sqrt{a^L}/2 & \sigma^L - \imath b^L & 0 \\ -\imath\sqrt{a^R}/2 & 0 & \sigma^R - \imath b^R \end{pmatrix}. \quad (2.17)$$

In this thesis, the generalized Floquet approach are employed as a nonperturbative treatment of the time-periodic non-Hermitian matrix Eq. 2.17 (or the generalized Hamiltonian). The generalized time-dependent Schrödinger equationEq. (2.16) may be effectively considered as the governing time-dependent equation of a single function LSD electrode-SQD-electrode system. The periodically driven SQD level (endowed with the on-site energy ϵ_0 and external field $A(t)$, $A(t+T) = A(t)$) is coupled (with the coupling amplitudes $\sqrt{a^L}/2$ and $\sqrt{a^R}/2$) to two unstable levels (endowed with the energies σ^L and σ^R and widths b^L and b^R, respectively, mimicking the spectral densities of state in the left and right electrodes), see Fig. 2.2

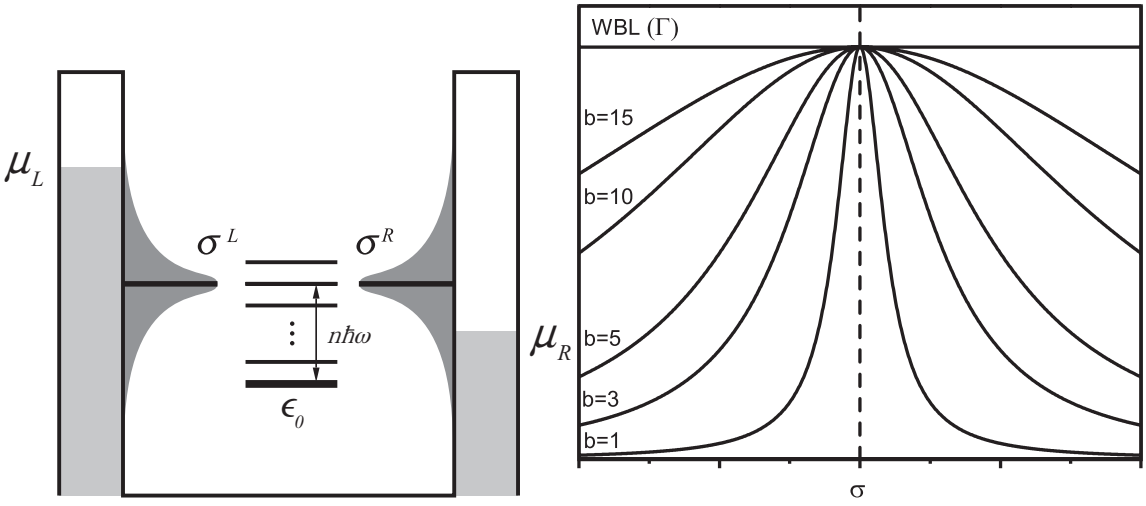

Figure 2.2: Energy diagram of the SQD driven by a periodic external field with frequency ω. The shade area represent the single Lorentzian spectral density located at the center: σ^L and σ^R. The thin levels are corresponding to the PAT sidebands generated by the external filed. The left panel shows the Lorentzian spectral density at various finite widths.

The corresponding energy diagram are shown in the Fig. 2.2 with the thick line indicating the energy level ϵ_0 in the SQD and the shaded region representing the single Lorentzian spectral density at position $\sigma^L = \sigma^R$. The left panel show the relation of single Lorentzian functions for various finite band widths with respect to the WBL ($\bar{\Gamma}(\epsilon) \to \Gamma$). The thin lines indicate the PAT side bands for ($\epsilon_0 + m\hbar\omega$) generated by the external fields.

2.3 Floquet formulation

Following the review in [37], we introduce and formulate the Floquet theory that will be implemented in this thesis. Let us consider some general properties of the wave functions of a time-periodic driven quantum system with period T ($\omega = 2\pi/T$). The system can be expressed as

$$\hat{H}(r,t) = \hat{H}_0(r) + \hat{V}(r,t) \tag{2.18}$$

where $\hat{V}(r,t) = \hat{V}(r,t+T)$. The eigenfunctions of the unperturbed Hamiltonian, denoted as $|\alpha(r)\rangle$, construct a complete orthonormal basis satisfy:

$$\hat{H}_0(r)|\alpha(r)\rangle = E^0_\alpha|\alpha(r)\rangle, \;\; \langle\alpha'(r)|\alpha(r)\rangle = \delta_{\alpha\alpha'} \tag{2.19}$$

According to the Floquet theorem [34], there exist a complete set of solutions of the form, (called the quasi-energy states (QES))

$$|\Psi_\beta(r,t)\rangle = \mathrm{e}^{-\imath\lambda_\beta t/\hbar}|\Phi_\beta(r,t)\rangle, \tag{2.20}$$

where $|\Phi_\beta(r,t)\rangle$ is a time-periodic state ($|\Phi_\beta(r,t)\rangle = |\Phi_\beta(r,t+T)\rangle$) and the quasi-energy λ_β is a real parameter in conventional Floquet theorem. However, the quasi-energy in the generalized Floquet theory can be complex. Hence, the Schrödinger equation is equivalent to the eigenvalue equation,

$$\left\{\hat{H}(r,t) - \imath\hbar\frac{\partial}{\partial t}\right\}|\Phi_\beta(r,t)\rangle = \lambda_\beta|\Phi_\beta(r,t)\rangle. \tag{2.21}$$

Due to the time-periodicity, for an arbitrary integer m, the following transformation

$$\begin{cases} \lambda'_\beta = \lambda_\beta + m\hbar\omega \\ |\Phi'_\beta(r,t)\rangle = \mathrm{e}^{\imath m\omega t}|\Phi_\beta(r,t)\rangle \end{cases} \tag{2.22}$$

still satisfy the eigenvalue equation, c.f. Eq. (2.21).

Since $|\Phi_\beta(r,t)\rangle = |\Phi_\beta(r,t+T)\rangle$, it can be expanded as a Fourier series

$$|\Phi_\beta(r,t)\rangle = \sum_\alpha \sum_{n=-\infty}^{\infty} \Phi^{(n)}_{\alpha\beta}|\alpha(r)\rangle \times \mathbf{e}^{-\imath n\omega t}, \tag{2.23}$$

where $\Phi_{\alpha\beta}^{(n)}$ is the Fourier coefficient of $\langle\alpha(r)|\Phi_\beta(r,t)\rangle$. Thus, the QES can be written as

$$|\Psi_\beta(r,t)\rangle = \sum_\alpha \sum_{n=-\infty}^{\infty} \Phi_{\alpha\beta}^{(n)} |\alpha(r)\rangle \times \mathbf{e}^{-\imath(\lambda_\beta + n\hbar\omega)t/\hbar}, \tag{2.24}$$

which is a linear combination of stationary states with energies $\lambda_\beta + n\hbar\omega$. Substituting Eq. (2.24) into Eq. (2.21), we obtain a set of time-independent coupled equations:

$$\sum_\alpha \sum_{n=-\infty}^{\infty} [\hat{H}_{\alpha\beta}^{(m-n)} - (\lambda_\beta + m\hbar\omega)\delta_{mn}\delta_{\alpha\beta}]\Phi_{\alpha\beta}^{(n)} = 0 \tag{2.25}$$

where $\hat{H}_{\alpha\beta}^{(m-n)} = \langle\alpha(r)|\hat{H}^{(m-n)}(r)|\beta(r)\rangle$ and

$$\hat{H}^{(m-n)}(r) \equiv \frac{1}{T}\int_0^T \hat{H}(r,t) \times \mathbf{e}^{\imath(m-n)\omega t} dt \tag{2.26}$$

We may introduce the Floquet state nomenclature by denoting the stationary states as $|\alpha n\rangle \equiv |\alpha\rangle \otimes |n\rangle$, such that $\langle r|\alpha\rangle = |\alpha(r)\rangle$ and $\langle t|n\rangle = \mathbf{e}^{\imath n\omega t}$. Hence, in terms of Floquet states, we can recast Eq. (2.25) into a infinite-dimensional eigenvalue equation:

$$\sum_\gamma \sum_{k=-\infty}^{\infty} \langle\alpha n|\hat{H}_F|\gamma k\rangle \Phi_{\gamma\beta}^{(k)} = \lambda_\beta \Phi_{\alpha\beta}^{(n)} \tag{2.27}$$

where $\hat{H}_F$ is the time-independent infinite-dimensional Floquet Hamiltonian whose matrix elements are

$$\langle\alpha n|\hat{H}_F|\gamma k\rangle = \hat{H}_{\alpha\gamma}^{(n-k)} + n\hbar\omega\delta\alpha\gamma\delta_{nk}. \tag{2.28}$$

Eq. 2.27 is the working equation of the Floquet calculation. In practical implementation, we need to truncate the matrix size of the Floquet Hamiltonian to get converged results.

Chapter 3

Generalized Floquet approach for the single LSD

3.1 Non-Hermitian Floquet matrix formalism

In this chapter, we implement the Floquet formulation in the chapter 2. To facilitate the derivations, Eq. (2.16) can be rewritten as

$$\imath\hbar\frac{d}{dt}|\Psi(t)\rangle = \mathcal{H}(t)|\Psi(t)\rangle,\ |\Psi(t_0)\rangle = \begin{pmatrix} 1 \\ 0 \\ 0 \end{pmatrix}, \tag{3.1}$$

where $\mathcal{H}(t+T) = \mathcal{H}(t)$ and the three-dimensional wave function $|\Psi(t)\rangle$ is defined as

$$|\Psi(t)\rangle = \begin{pmatrix} U(t,t_0) \\ Y^L(t,t_0) \\ Y^R(t,t_0) \end{pmatrix}. \tag{3.2}$$

By invoking the generalized Floquet approach [37] for the non-Hermittian matrix, the wave function $|\Psi(t)\rangle$ can be written as

$$|\Psi_\beta(t)\rangle = \mathbf{e}^{-\imath\lambda_{\beta 0}t/\hbar}|\Phi_\beta(t)\rangle, \tag{3.3}$$

where the quasi-energy state (QES) function $|\Phi_\beta(t)\rangle$, associated with the quasi-energy $\lambda_{\beta 0}$, is a periodic function of time, i. e. $|\Phi_\beta(t+T)\rangle = |\Phi_\beta(t)\rangle$, and satisfies the equation

$$\left\{\mathcal{H}(t) - \imath\hbar\frac{d}{dt}\right\}|\Phi_\beta(t)\rangle = \lambda_{\beta 0}|\Phi_\beta(t)\rangle. \tag{3.4}$$

The QES functions $|\Phi_\beta(t)\rangle$, $\beta = 1,2,3$, form a complete basis set.

The periodic quantities $\mathcal{H}(t)$ and $|\Phi_\beta(t)\rangle$ can be expanded as

$$\mathcal{H}(t) = \sum_{n-\infty}^{\infty}\mathcal{H}^{(n)}\mathbf{e}^{\imath n\omega t}, \tag{3.5}$$

and

$$|\Phi_\beta(t)\rangle = \sum_{\alpha=1}^{3}\sum_{n=-\infty}^{\infty}|\alpha\rangle\langle\alpha n|\lambda_{\beta 0}\rangle\mathbf{e}^{\imath n\omega t},\ \beta = 1,2,3, \tag{3.6}$$

respectively, where $|\alpha\rangle$, $\alpha = 1,2,3$, are the field-free eigen states of $\mathcal{H}(t)$ with $A(t) = 0$. By resorting to the Fourier expansions Eqs. (3.5) and (3.6), the time dependent equation Eq. (3.4) can be cast as an infinite-dimensional time-independent quasi-energy prob-

lem

$$\sum_{\beta=1}^{3}\sum_{n=-\infty}^{\infty}\left\{\langle\alpha|\mathcal{H}^{(m-n)}|\beta\rangle+m\hbar\omega\delta_{\alpha\beta}\delta_{mn}\right\}\langle\beta n|\lambda_{\gamma k}\rangle=\lambda_{\gamma k}\langle\alpha m|\lambda_{\gamma k}\rangle, \tag{3.7}$$

for $\gamma=1,2,3,\ k=-\infty,\cdots,\infty$. For the non-Hermittian matrix, its concomitant adjoint eigenvalue problem

$$\sum_{\beta=1}^{3}\sum_{n=-\infty}^{\infty}\left\{\langle\alpha|\left[\mathcal{H}^{(m-n)}\right]^{\dagger}|\beta\rangle+m\hbar\omega\delta_{\alpha\beta}\delta_{mn}\right\}\langle\beta n|\bar{\lambda}_{\gamma k}\rangle=\bar{\lambda}_{\gamma k}\langle\alpha m|\bar{\lambda}_{\gamma k}\rangle \tag{3.8}$$

for $\gamma=1,2,3,\ k=-\infty,\cdots,\infty$. Here the eigen-solutions of Eqs. (3.7) and (3.8) possess the properties[37]: the quasi-energy is

$$\bar{\lambda}^{*}_{\beta n}=\lambda_{\beta n}=\lambda_{\beta 0}+n\hbar\omega, \tag{3.9}$$

; the eigenstates are orthogonal and complete,

$$\langle\bar{\lambda}_{\alpha m}|\lambda_{\beta n}\rangle=\delta_{\alpha\beta}\delta_{mn}, \tag{3.10}$$

$$\sum_{\beta=1}^{3}\sum_{n=-\infty}^{\infty}|\lambda_{\beta n}\rangle\langle\bar{\lambda}_{\beta n}|=\mathbf{I}, \tag{3.11}$$

and also periodic

$$\langle\alpha,m+\ell|\lambda_{\beta n+\ell}\rangle=\langle\alpha m|\lambda_{\beta n}\rangle, \tag{3.12}$$

and

$$\langle\alpha,m+\ell|\bar{\lambda}_{\beta n+\ell}\rangle=\langle\alpha m|\bar{\lambda}_{\beta n}\rangle. \tag{3.13}$$

The matrix elements of the propagator $\mathcal{U}(t,t_0)$, a 3×3 matrix function, of Eq. (3.1) can then be written in terms of eigen-solutions of Eqs. (3.7) and (3.8). Given the initial

condition of Eq. (3.1), we have $U(t,t_0) = \mathcal{U}_{11}(t,t_0)$, which leads to the underlying single particle propagator:

$$U(t,t_0) = \sum_{\beta=1}^{3}\sum_{m=-\infty}^{\infty}\sum_{n=-\infty}^{\infty}\langle\alpha=1,m|\lambda_{\beta 0}\rangle\langle\bar{\lambda}_{\beta 0}|\alpha=1,n\rangle \mathbf{e}^{-\imath\lambda_{\beta 0}(t-t_0)/\hbar}\mathbf{e}^{\imath(m\omega t - n\omega t_0)}. \tag{3.14}$$

By substituting Eq. (3.14) into Eqs. (2.3) and (2.4), the k-th Fourier coefficient of the retarded Green's function can be expressed explicitly as

$$G^{(k)}(\epsilon) = \sum_{\beta=1}^{3}\sum_{n=-\infty}^{\infty}\frac{\langle\alpha=1,-k|\lambda_{\beta n}\rangle\langle\bar{\lambda}_{\beta n}|\alpha=1,0\rangle}{\epsilon-\lambda_{\beta 0}-n\hbar\omega}. \tag{3.15}$$

As a result, the total transmission coefficient, Eq. (2.6), can be expressed as

$$T_{LR/RL}(\epsilon) = \frac{1}{4}\sum_{k=-\infty}^{\infty}\bar{\Gamma}_{L/R}(\epsilon+k\hbar\omega)\bar{\Gamma}_{R/L}(\epsilon)\left|\sum_{\beta=1}^{3}\sum_{n=-\infty}^{\infty}\frac{\langle\alpha=1,-k|\lambda_{\beta n}\rangle\langle\bar{\lambda}_{\beta n}|\alpha=1,0\rangle}{\epsilon-\lambda_{\beta 0}-n\hbar\omega}\right|^2, \tag{3.16}$$

which can in turn be used to obtain the d.c. current based on Eq. (2.7).

3.2 Transmission coefficient profiles

We implement the generalized Floquet approach and calculated all the Floquet and its corresponding quasi-energy by numerically solving the eigenvalue problem, Eq. (3.7) and (3.8). The converged numerical calculation are carried out with a truncated Floquet Hamiltonian. The frequency of the driving field $A(t) = A\cos\omega t$ is fixed at $\hbar\omega = 10\,eV$, which is adopted as the unit of energy.The symmetric single function LSDs for the left and right electrodes possess the same peak center at $\sigma^L = \sigma^R = \sigma = 0$ and the same width of $b^L = b^R = b$. Moreover, the spectral density in the WBL is chosen as $\Gamma^L = \Gamma^R = \Gamma = 0.1\ \hbar\omega$.

Thus, the transmission coefficient are also symmetric, $T_{LR}(\epsilon) = T_{RL}(\epsilon) = T(\epsilon)$

We first study the memory effect on the total transmission coefficient profiles by its profiles, i.e. $T(\epsilon)$ as a function of ϵ and the external field amplitude A, using Eq. (3.16). As Fig. 3.1 shown, manifest PAT sidebands structure can be observed as distinct channels (in the light color) at $\epsilon = k\hbar\omega$ for $k = 0, \pm1, \pm2, ...$ The PAT sidebands are corresponding to electron transport with multi-photon processes involved. In addition, as the amplitude increase, the external field will generate more PAT sidebands.

The upper panels shows the multi-photon processes in the WBL for (a) $\epsilon_0 = 0$ and (b) $\epsilon_0 = 2\hbar\omega$. Since the spectral density is energy-independent for the WBL, the entire profile merely shift without changing its structure. For the narrow LSD width ($b = 2\hbar\omega$), the lower panels represent the corresponding profiles: (c) $\epsilon_0 = \sigma = 0$ and (d) $\epsilon_0 = \sigma - 2\hbar\omega$ ($\sigma = 0$). As a result, the narrow LSD width turns out that the magnitude of higher order (larger $|k|$) PAT sidebands are suppressed and the width of PAT sideband is narrowed in general. In addition, the structure of PAT sidebands are not simply a shift and become non-symmetric, because the spectral density center is not coincided with on-site energy. Dominant electron transport through the 2-photon inelastic tunneling.

3.3 Current stair-step and Low-bias coherent destruction of tunneling

After we calculated the total transmission coefficient by 3.16, the d.c. current can be obtain by carrying out the integration in Eq. (2.7). The distinct peak structure of the total transmission coefficient results in the d.c. current jumping (stair-steps) when we vary the

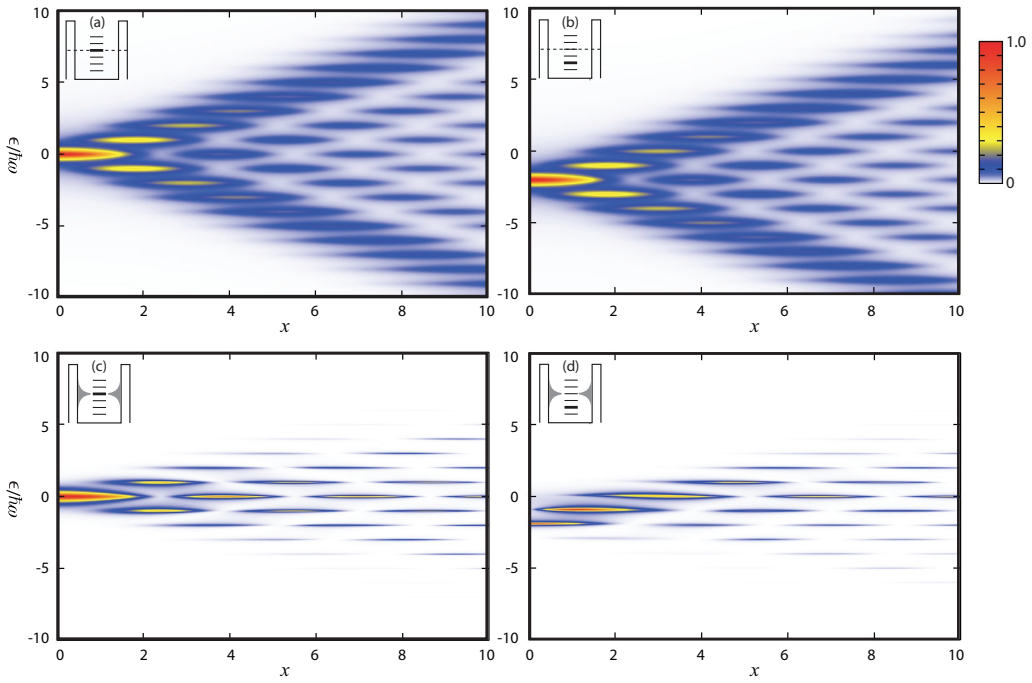

Figure 3.1: A contour map of the total transmission coefficient $T(\epsilon)$ are plotted as a function of ϵ and $x = A/\hbar\omega$ for (a) wide band limit with $\epsilon_0 = 0$ and (b) wide band limit with $\epsilon_0 = 2\hbar\omega$; (c) $b = 2\hbar\omega$ with $\epsilon_0 = 0$ and (d) $b = 2\hbar\omega$ with $\epsilon_0 = 2\hbar\omega$. The inserts show the corresponding energy diagrams.

bias voltage window.

For simplicity, we just consider the zero temperature limit. Figure 3.2 shows the relationship between (a) the stair-step feature of the d.c. current $\bar{I}$, as a function of μ_R (for $\mu_L = 0$) and (b) the PAT peak structure of the underlying transmission coefficient $T(\epsilon)$, a function of ϵ. The d.c. current stair steps result from the increasing number of the partial current associated with the peaks lying within the bias voltage window $[\mu_L, \mu_R]$ of the electrodes. Each peaks of the transmission coefficient is corresponding to a d.c. current jump in the upper panel. In addition, the narrower the peak is, the sharper the current jumps. We also compare the WBL results (the dashed curves) and the finite width ($b = 1\ \hbar\omega$) result. It is found, especially from the inset in the upper panel, that the d.c. current stair step become smoothed out in the WBL. In general, there are more non-vanishing PAT peaks contributing to the corresponding d.c. current in the WBL as the bias voltage

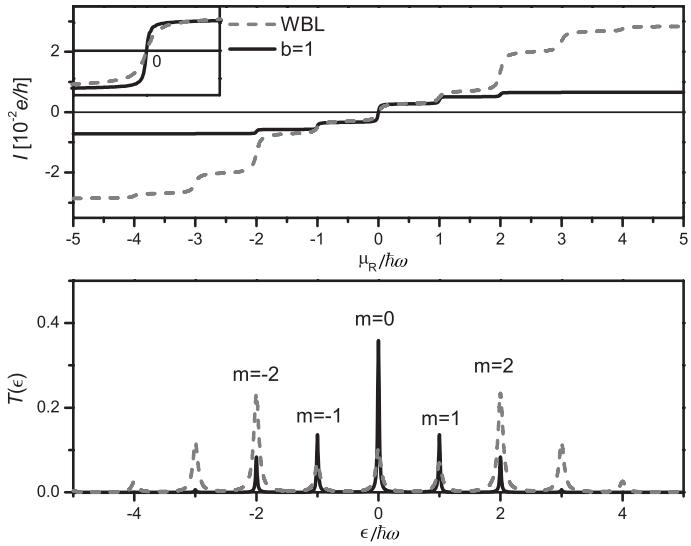

Figure 3.2: The d.c. current $\bar{I}$ is plotted as a function of the right Fermi energy μ_R with fixed $\mu_L = 0$ in the upper panel and its corresponding transmission coefficient is shown in the lower panel. We assume that $\epsilon_0 = \sigma = 0$. The finit width results for $b = 1\hbar\omega$ is compared with the WBL results (thick gray line). The stair steps of the d.c. current are correspond to the peaks of the transmission coefficient.

window $[\mu_L, \mu_R]$ becomes bigger. As the last section implied, the finite electrode spectral density width suppresses the higher-order (i.e., larger $|m|$) PAT sidebands more quickly, thus, leading to a much smaller d.c. current, when compared to the WBL counterpart, at a larger bias voltage window.

The coherent destruction of tunneling (CDT) phenomena infer to the complete vanishment of the d.c. current for certain $A/\hbar\omega$ ratio of the external field. In the case of the small bias voltage (voltage window include only one PAT sideband), CDT phenomena for one site coupled to reservoirs has been observed [28]. It was found that the coupling between the site and reservoir can be suppressed if the amplitude of the external field is chosen properly.

In our formulation, CDT of the small-bias voltage is predictable from the total transmission coefficient and, furthermore, we can observe the multi-photon (MP-) CDT [32] in some chosen situation. Here, we assume bias voltage is small ($\mu_L = -\mu_R = 0.1\hbar\omega$)

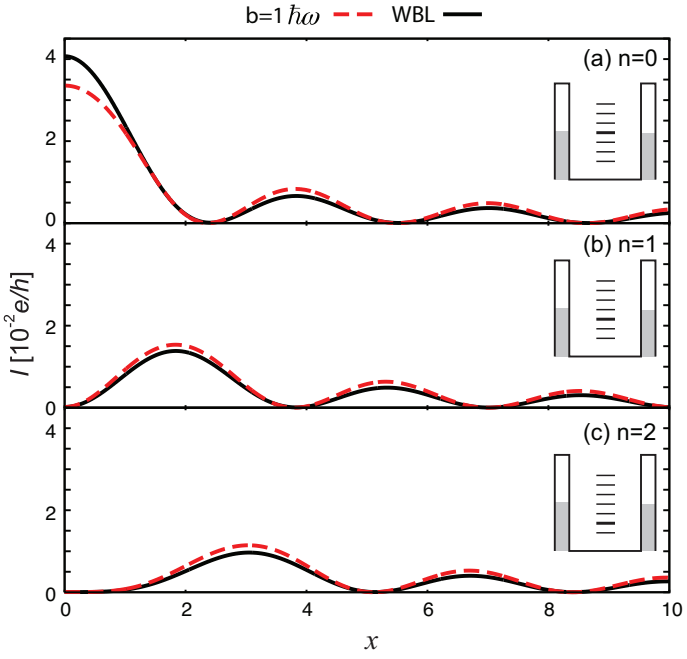

Figure 3.3: The d.c. current as a function of the external field amplitude $x = A/\hbar\omega$ for the WBL (black solid lines) and the finite width, $b = 1\hbar\omega$, (red dash lines). The panels are with respect to different on-site energies: $\epsilon_0 = \sigma + n\hbar\omega$ for (a) $n = 0$, (b) $n = 1$ and (c) $n = 2$.

which enclose only one PAT sideband. Therefore, the d.c. current only depends on the contribution of certain sideband enclosed in the voltage window. The Fig 3.1 reveals that the transmission coefficient vanish when $x = A/\hbar\omega$ are the roots of Bessel function of first kind. In Fig. (3.3), 1- and 2- photon CDT are also presented in panel (b) and (c) for $\epsilon_0 = -1\hbar\omega, -2\hbar\omega$, respectively. The d.c. current are completely destructed at the roots of $J_1(x)$ and $J_2(x)$. In addition, since the bias voltage is so small (smaller than the LSD width) that the current for finite LSD width is quite similar to the WBL results.

On the other hand, Fig. (3.4) explain why the CDT phenomena occur only for the small bias voltage. When increasing the bias voltage, more than one PAT sidebands will be included in the voltage window, i.e. more than one channels participate the electron transport. As the bias voltage increase, $e\mathbf{V} = 1, 3, 5, 7\hbar\omega$, the d.c. current rise for both WBL and finite band width. It is shown in the Fig. (3.1) that there are no two channels

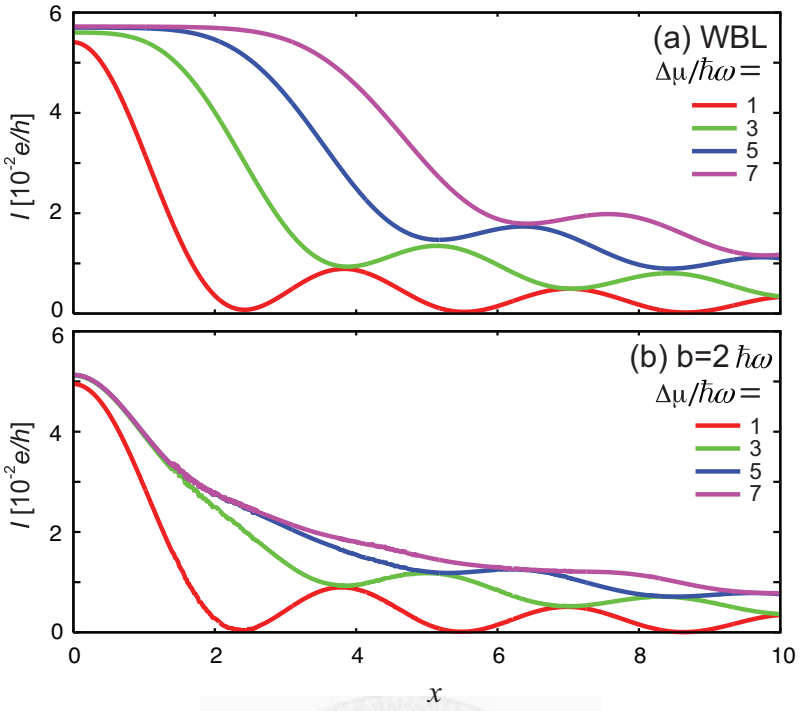

Figure 3.4: The d.c. current $\bar{I}$ is plotted to the dependence on the external field amplitude $x = A/\hbar\omega$. Here, we assume the resonant condition $\epsilon_0 = \sigma = 0$ and $\mu_L = -\mu_R = e\mathbf{V}/2$. As the bias voltage increase, $e\mathbf{V} = 1, 3, 5, 7\hbar\omega$, the d.c. current rise for both The current are shown in the panel (a) for the WBL and (b) for finite width $b = 2\hbar\omega$.

both vanish at the same amplitude, which imply that CDT should not occur if more than one channels participate. Even for the finite width (here, $b = 2\hbar\omega$), the contribution of additional sidebands are only suppressed, rather than vanish.

3.4 Large-bias blockade phenomena

We then study the memory effect on the electron tunneling blockade phenomenon at different external field amplitudes A of the applied field $A(t)$, by specifically calculating the d.c. current $\bar{I}$ as a function of the gate voltage ϵ_0, in two limiting cases: (a) at a near zero bias voltage of $\mu_L = -\mu_R = 0.1\ \hbar\omega$ in the WBL, Fig. 3.5a, and (b) at a large bias voltage of $\mu_L = -\mu_R = 10\ \hbar\omega$ for a narrow band width $b = 1\ \hbar\omega$, Fig. 3.5b. In the low bias voltage Coulomb blockade (CB) regime, i.e. $\mu_L \sim \mu_R$, (Fig. 3.5a), the number of the d.c.

current CB sidebands increases with the amplitude A, due to the tunneling induced by the absorption and emission of multiple photons, as indicated by the PAT processes [10]. Around the zero bias voltage, electrons in the electrodes can tunnel through the SQD only when one of the sideband generated by the external field resides inside the bias voltage window. In this limit case, the finite band effect is not obvious since the bias voltage window is much smaller than the LSD width. The pump current (defined as the d.c. current difference $\bar{I} - \bar{I}_0$, with $\bar{I}$ and $\bar{I}_0$, respectively, for a non-zero and zero external field) oscillation as a function of ϵ_0 occurring around the zero bias voltage is commonly observed for small applied field amplitudes in the WBL, and is closely related to the PAT in the absence of the symmetric applied field [4].

On the other hand, in the large bias voltage regime (Fig. 3.5b), significant oscillatory Coulomb blockade features in the pump current $\bar{I} - \bar{I}_0$ are also observed, as seen in Fig. 3.5c. In the WBL, the d.c. current for very large bias voltage ($\mu_L = -\mu_R \to \infty$) can be computed explicitly as (see chapter 5)

$$\bar{I}_\infty = \frac{e}{h}\frac{\pi\Gamma}{2}, \tag{3.17}$$

which depends only on the coupling strength Γ. Here $\Gamma = 0.1\hbar\omega$, thus, $\bar{I}_\infty = 5.772 \times 10^{-2}\ [e/h]$. However, by including the memory effect, the tunneling current could be effectively blocked between the SQD and the electrode because of the limited accessible energy bandwidth in the single function LSD model of the electrodes. The tunneling coupling between the SQD and the electrodes is strongest when the on-site energy ϵ_0 coincides with σ, see the inset in Fig. 3.5(b). The coupling falls off to zero quickly as soon as ϵ_0 is moved outside the designated band width b, leading to the d.c. current Coulomb blockade.

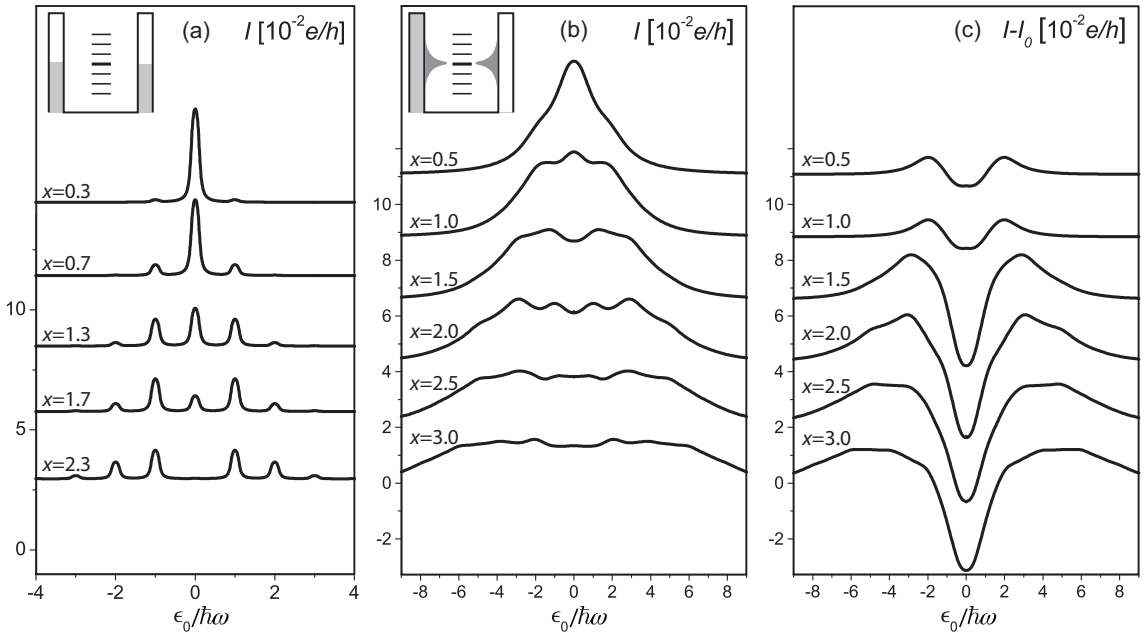

Figure 3.5: The d.c. currents $\bar{I}$ and the pumped current $\bar{I} - \bar{I}_0$ are shown as a function of energy level (ϵ_0). We plot the d.c. current a a function of the gate voltage ϵ_0: (a) around zero bias voltage ($\mu_L = -\mu_R = 0.1\ [\hbar\omega]$) in the WBL and (b) for large voltage ($\mu_L = -\mu_R = 10\ [\hbar\omega]$) for a narrow bandwidth $b = 1\ [\hbar\omega]$. Under the same set-up with (b), we also plot the pumped current to reveal the current oscillation in the panel (c). The insets represent the corresponding energy diagrams.

The two bias voltage regimes considered in Fig. 3.5 clearly reveals two different mechanisms for the d.c. current Coulomb blockade phenomena – one associated with very small bias voltages in the WBL and the other with very large bias voltages while including the memory effect (here with a narrow band width). The interplay of the band width b and the bias voltage window $[\mu_L, \mu_R]$ may result in the enhancement or suppression of the d.c. current by manipulating the gate voltage ϵ_0.

Chapter 4

Nearly-degenerate generalized Van Vleck perturbation approach

4.1 Formulation for symmetric single LSD

It is of particular interest to study the case of the symmetric single function LSD model in which $\sigma^L = \sigma^R = \sigma$, $b^L = b^R = b$, and $a^L = a^R = a$, see Fig. 2. In this case, Eq. (2.16) can be further reduced to a two-dimensional coupled equation, i.e.,

$$\imath\hbar\frac{d}{dt}\begin{pmatrix} U(t,t_0) \\ \\ Y^+(t,t_0) \end{pmatrix} = \tilde{\mathcal{H}}(t)\begin{pmatrix} U(t,t_0) \\ \\ Y^+(t,t_0) \end{pmatrix}, \tag{4.1}$$

where

$$Y^{\pm}(t,t_0) = (Y^R(t,t_0) \pm Y^L(t,t_0))/\sqrt{2}, \tag{4.2}$$

and

$$\tilde{\mathcal{H}}(t) = \begin{pmatrix} \epsilon_0 + A\cos\omega t & \imath\sqrt{a/2} \\ -\imath\sqrt{a/2} & \sigma - \imath b \end{pmatrix}, \tag{4.3}$$

assuming explicitly that $A(t) = A\cos\omega t$. Here it is remarked that $Y^-(t, t_0) = 0\ \forall t \geq t_0$ since it is decoupled from both $U(t, t_0)$ and $Y^+(t, t_0)$ and the initial condition $Y^-(t_0, t_0) = 0$. Accordingly, the single function LSD response function can be written as

$$\bar{\Gamma}_L(\epsilon) = \bar{\Gamma}_R(\epsilon) = \bar{\Gamma}(\epsilon) = \frac{ab}{\epsilon^2 + b^2} = \Gamma\frac{b^2}{\epsilon^2 + b^2}, \tag{4.4}$$

where $\Gamma = a/b$, resulting in the same expression for both the transmission coefficients, i. e.,

$$T_{RL}(\epsilon) = T_{LR}(\epsilon) = T(\epsilon) = \frac{1}{4}\sum_k \bar{\Gamma}(\epsilon + k\hbar\omega)\bar{\Gamma}(\epsilon)|G^{(k)}(\epsilon)|^2, \tag{4.5}$$

and a simple form for the d.c. current

$$\bar{I} = \frac{e}{h}\int_{-\infty}^{\infty} T(\epsilon)[f_R(\epsilon) - f_L(\epsilon)]d\epsilon, \tag{4.6}$$

which is further reduced to

$$\bar{I} = \frac{e}{h}\int_{\mu_R}^{\mu_L} T(\epsilon)d\epsilon, \tag{4.7}$$

at the zero temperature. The transmission coefficient $T(\epsilon)$ is further reduced to

$$T_{WBL}(\epsilon) = \frac{1}{4}\Gamma^2\sum_k |G^{(k)}(\epsilon)|^2, \tag{4.8}$$

in the WBL, since $\bar{\Gamma}(\epsilon) \to \Gamma = a/b$ in the limit of $b \to \infty$, cf. Eq. (4.4).

Here, the energy level are assumed to satisfy the near resonance condition $\epsilon_0 \approx \sigma -$

$n\hbar\omega$ that we can facilitate the nearly-degenerate perturbation treatment in the next section.

4.2 Nearly-degenerate GVV perturbation

In the near resonance condition $\epsilon_0 \approx \sigma - n\hbar\omega$, it is expedient to transform Eq. (4.1) into an n-th order resonance rotating frame via the transformation

$$\mathcal{R}_n(t) = \begin{pmatrix} \mathrm{e}^{-\imath\Theta(t)/\hbar} & 0 \\ 0 & \mathrm{e}^{-\imath n\omega t} \end{pmatrix}, \tag{4.9}$$

where $\Theta(t) = \int^t A(t')dt' = \frac{A}{\omega}\sin\omega t$. The rotated state

$$\begin{pmatrix} U'(t,t_0) \\ Y'(t,t_0) \end{pmatrix} = \mathcal{R}_n^{-1}(t) \begin{pmatrix} U(t,t_0) \\ Y^+(t,t_0) \end{pmatrix}, \tag{4.10}$$

satisfies the equation

$$\imath\hbar\frac{\partial}{\partial t}\begin{pmatrix} U'(t,t_0) \\ Y'(t,t_0) \end{pmatrix} = \mathcal{H}'(t)\begin{pmatrix} U'(t,t_0) \\ Y'(t,t_0) \end{pmatrix}, \quad \begin{pmatrix} U'(t_0,t_0) \\ Y'(t_0,t_0) \end{pmatrix} = \begin{pmatrix} 1 \\ 0 \end{pmatrix}, \tag{4.11}$$

where the rotated Hamiltonian is

$$\mathcal{H}'(t) = \begin{pmatrix} \epsilon_0 & \imath\xi\sum_m J_{n-m}(x)\mathbf{e}^{-\imath m\omega t} \\ -\imath\xi\sum_m J_{n+m}(x)\mathbf{e}^{-\imath m\omega t} & \sigma - n\hbar\omega - \imath b \end{pmatrix}. \tag{4.12}$$

We adapt $\xi = \sqrt{\Gamma b/2}$ as the perturbation parameter that is valid for the weak coupling and finite band width. Here, we have used the relation

$$\mathrm{e}^{\imath x \sin \omega t} = \sum_{m=-\infty}^{\infty} J_m(x) \mathrm{e}^{\imath m \omega t}. \tag{4.13}$$

The rotated Hamiltonian are featured by the n-photons resonance condition in its diagonal terms that leads to an effective non-Hermitian two-levels system and the off-diagonal terms are composed of multiple photons process couplings ($\mathbf{e}^{-\imath m \omega t}$), which represents the absorption or emission of $|m|$ photons , with Bessel function coefficient $J_{n \pm m}(x)$. Thus, two different photon-assisted processes are included: n photon resonance between the SQD (ϵ_0) and the LSD peak position (σ), and, m-photon inelastic scattering processes. It can be shown that the evolution propagator $\mathcal{U}(t, t')$ of Eq. (4.1) can be written as

$$\mathcal{U}(t, t') = \mathcal{R}_n(t) \mathcal{U}'(t, t') \mathcal{R}_n^{-1}(t'), \tag{4.14}$$

where $\mathcal{U}'(t, t')$ is the evolution propagator for Eq. (4.11) in the rotating frame.

The infinite-dimensional time-independent Floquet Hamiltonian corresponding to the time-dependent equation Eq. (4.11), in the n-th order resonance rotating frame, can be expressed as

$$\mathbf{H}_F = \mathbf{H}_0 + \mathbf{V}, \tag{4.15}$$

where

$$\mathbf{H}_0 = \begin{pmatrix} \ddots & & & & & & \\ & \mathcal{H}_n^{(0)} + 2\hbar\omega\mathcal{I} & 0 & 0 & 0 & 0 & \\ & 0 & \mathcal{H}_n^{(0)} + \hbar\omega\mathcal{I} & 0 & 0 & 0 & \\ & 0 & 0 & \mathcal{H}_n^{(0)} & 0 & 0 & \\ & 0 & 0 & 0 & \mathcal{H}_n^{(0)} - \hbar\omega\mathcal{I} & 0 & \\ & 0 & 0 & 0 & 0 & \mathcal{H}_n^{(0)} - 2\hbar\omega\mathcal{I} & \\ & & & & & & \ddots \end{pmatrix}, \tag{4.16}$$

and

$$\mathbf{V} = \begin{pmatrix} \ddots & & & & & \\ & 0 & \mathcal{V}_n^{(1)} & \mathcal{V}_n^{(2)} & \mathcal{V}_n^{(3)} & \mathcal{V}_n^{(4)} & \\ & \mathcal{V}_n^{(-1)} & 0 & \mathcal{V}_n^{(1)} & \mathcal{V}_n^{(2)} & \mathcal{V}_n^{(3)} & \\ & \mathcal{V}_n^{(-2)} & \mathcal{V}_n^{(-1)} & 0 & \mathcal{V}_n^{(1)} & \mathcal{V}_n^{(2)} & \\ & \mathcal{V}_n^{(-3)} & \mathcal{V}_n^{(-2)} & \mathcal{V}_n^{(-1)} & 0 & \mathcal{V}_n^{(1)} & \\ & \mathcal{V}_n^{(-4)} & \mathcal{V}_n^{(-3)} & \mathcal{V}_n^{(-2)} & \mathcal{V}_n^{(-1)} & 0 & \\ & & & & & & \ddots \end{pmatrix}, \tag{4.17}$$

with $\mathcal{I}$ being a 2×2 identity matrix. Here $\mathbf{H}_0$ and $\mathbf{V}$ are, respectively, composed of 2×2 sub-blocks

$$\mathcal{H}_n^{(0)} = \begin{pmatrix} \epsilon_0 & 0 \\ 0 & \sigma - n\hbar\omega - \imath b \end{pmatrix}, \tag{4.18}$$

and

$$\mathcal{V}_n^{(m)} = \imath\xi \begin{pmatrix} 0 & J_{n-m}(x) \\ -J_{n+m}(x) & 0 \end{pmatrix}, \tag{4.19}$$

with $\xi = \sqrt{\Gamma b/2}$ and $\epsilon_0 \approx \sigma - n\hbar\omega$.

The main idea of GVV perturbation theory is to project the infinite-dimensional matrix into a finite matrix using perturbation method as some effective terms. By invoking the nearly degenerate GVV perturbation theory, an effective n-photon resonant 2×2 Hamiltonian $\mathcal{H}_n$ and its two eigenstates $|\varphi_{n\pm}\rangle$ can be, respectively, expanded as power series of ξ

$$\mathcal{H}_n = \mathcal{H}_n^{(0)} + \sum_{m=1}^{\infty} \xi^m \mathcal{H}_n^{(m)}, \tag{4.20}$$

and

$$|\varphi_{n\pm}\rangle = \sum_{m=0}^{\infty} \xi^m |\varphi_{n\pm}^{(m)}\rangle. \tag{4.21}$$

Since $\mathcal{H}_n^{(0)}$ is diagonal, the unperturbed eigenstates are

$$|\varphi_{n+}^{(0)}\rangle = |\alpha = 1, 0\rangle, \tag{4.22}$$

and

$$|\varphi_{n-}^{(0)}\rangle = |\alpha = 2, 0\rangle, \tag{4.23}$$

respectively. We derive the first order perturbation of $\mathcal{H}_n$,

$$\mathcal{H}_n^{(1)} = \begin{pmatrix} \langle\varphi_{n+}^{(0)}|\mathbf{V}|\varphi_{n+}^{(0)}\rangle & \langle\varphi_{n+}^{(0)}|\mathbf{V}|\varphi_{n-}^{(0)}\rangle \\ \langle\varphi_{n-}^{(0)}|\mathbf{V}|\varphi_{n+}^{(0)}\rangle & \langle\varphi_{n-}^{(0)}|\mathbf{V}|\varphi_{n-}^{(0)}\rangle \end{pmatrix} = \begin{pmatrix} 0 & \imath J_n(x) \\ -\imath J_n(x) & 0 \end{pmatrix}, \tag{4.24}$$

and the first perturbation of eigenstates $|\varphi_{n\pm}\rangle$,

$$|\varphi_{n+}^{(1)}\rangle = \sum_{\alpha'} \sum_{m\neq 0} \frac{\langle\alpha', m|\mathbf{V}|\alpha = 0, 0\rangle}{\epsilon_0 - \langle\alpha', m|\mathbf{H}_0|\alpha', m\rangle} |\alpha', m\rangle = \sum_{m\neq 0} \frac{-\imath J_{n+m}(x)}{\imath b - m\hbar\omega} |\alpha = 2, m\rangle, \tag{4.25}$$

and

$$|\varphi_{n-}^{(1)}\rangle = \sum_{\alpha'}\sum_{m\neq 0}\frac{\langle\alpha',m|\mathbf{V}|\alpha=1,0\rangle}{\epsilon_0 - \imath b - \langle\alpha',m|\mathbf{H}_0|\alpha',m\rangle}|\alpha',m\rangle = \sum_{m\neq 0}\frac{\imath J_{n+m}(x)}{-\imath b - m\hbar\omega}|\alpha=1,m\rangle. \tag{4.26}$$

Furthermore, the second order perturbation of $\mathcal{H}_n^{(2)}$ of the effective Hamiltonian $\mathcal{H}_n$ can be derived as

$$\begin{aligned}\mathcal{H}_n^{(2)} &= \begin{pmatrix} \langle\varphi_{n+}^{(0)}|\mathbf{V}|\varphi_{n+}^{(1)}\rangle & \langle\varphi_{n+}^{(0)}|\mathbf{V}|\varphi_{n-}^{(1)}\rangle \\ \langle\varphi_{n-}^{(0)}|\mathbf{V}|\varphi_{n+}^{(1)}\rangle & \langle\varphi_{n-}^{(0)}|\mathbf{V}|\varphi_{n-}^{(1)}\rangle \end{pmatrix} - \mathcal{H}_n^{(1)}\begin{pmatrix} \langle\varphi_{n+}^{(0)}|\varphi_{n+}^{(1)}\rangle & \langle\varphi_{n+}^{(0)}|\varphi_{n-}^{(1)}\rangle \\ \langle\varphi_{n-}^{(0)}|\varphi_{n+}^{(1)}\rangle & \langle\varphi_{n-}^{(0)}|\varphi_{n-}^{(1)}\rangle \end{pmatrix} \\ &= \begin{pmatrix} -\delta_n & 0 \\ 0 & \delta_n \end{pmatrix},\end{aligned} \tag{4.27}$$

where

$$\delta_n = \sum_{m\neq 0}\frac{J_{n+m}^2(x)}{-\imath b + m\hbar\omega} = \begin{cases} \imath\sum_{m\neq 0}\frac{b}{(m\hbar\omega)^2+b^2}J_m^2(x) & \text{if} \quad n=0 \\ \sum_{m\neq 0}\frac{m\hbar\omega}{(m\hbar\omega)^2+b^2}J_{n+m}^2(x) + \imath\sum_{m\neq 0}\frac{b}{(m\hbar\omega)^2+b^2}J_{n+m}^2(x) & \text{if} \quad n\neq 0 \end{cases} \tag{4.28}$$

The n-photon GVV effective Hamiltonian, up to the second-order, can then take on the form

$$\mathcal{H}_{GVV}^{[n]} = \begin{pmatrix} \epsilon_0 - \xi^2\delta_n & \imath\xi J_n(x) \\ -\imath\xi J_n(x) & \epsilon_0 - \imath b + \xi^2\delta_n \end{pmatrix}, \tag{4.29}$$

compared to the corresponding n-photon effective Hamiltonian

$$\mathcal{H}_{RWA}^{[n]} = \begin{pmatrix} \epsilon_0 & \imath\xi J_n(x) \\ -\imath\xi J_n(x) & \epsilon_0 - \imath b \end{pmatrix}, \tag{4.30}$$

in the rotating wave approximation (RWA). The imaginary part of δ_n, together with the off-diagonal first order correction, result in the broadening or narrowing of the PAT peaks. On the other hand, the real part of δ_n is responsible for the level shift conventionally [58] that only occur for the resonance condition $n \neq 0$. Unlike the RWA effective Hamiltonian, the GVV effective Hamiltonian contain the level shift and higher order modification of the peak width.

It is shown in the above that by invoking the nearly degenerate GVV perturbation method, upon transforming the time-dependent equation Eq. (4.11) to a time-independent Floquet quasi-energy eigen-problem, Eq. (4.11) may be further approximated as

$$\imath\hbar\frac{\partial}{\partial t}\begin{pmatrix} U^{[n]}(t,t_0) \\ Y^{[n]}(t,t_0) \end{pmatrix} = \mathcal{H}^{[n]}_{GVV}\begin{pmatrix} U^{[n]}(t,t_0) \\ Y^{[n]}(t,t_0) \end{pmatrix}, \tag{4.31}$$

at the near resonance condition $\epsilon_0 \approx \sigma - n\hbar\omega$.

In the weak coupling limit ($\Gamma \ll \hbar\omega$), we derive the approximated eigenstates of Eq. 4.31 by the following. The eigenvalues of the GVV effective Hamiltonian $\mathcal{H}^{[n]}_{GVV}$ can be explicitly written as

$$\lambda^{[n]}_{\pm} = \epsilon_0 \pm \frac{\imath b}{2}\left(\sqrt{(1+\imath\Gamma\delta_n)^2 - 2\Gamma J_n^2(x)/b} \mp 1\right). \tag{4.32}$$

Then we take the approximation

$$\sqrt{(1+\imath\Gamma\delta_n)^2 - 2\Gamma\bar{J}_n^2/b} \mp 1 \approx \left(1 - \frac{2\Sigma_n}{b} + \imath\frac{2\Delta_n}{b}\right) \mp 1, \tag{4.33}$$

and obtain the approximated eigenvalues

$$\begin{cases} \lambda_{+}^{[n]} = \epsilon_0 - \Delta_n - \imath\Sigma_n \\ \lambda_{-}^{[n]} = \sigma - n\hbar\omega - \imath b + \Delta_n + \imath\Sigma_n. \end{cases} \tag{4.34}$$

where we have defined two parameters:

$$\Delta_n \equiv \begin{cases} 0 & \text{if} \quad n = 0 \\ \frac{\Gamma}{2} \sum\limits_{m \neq 0} \frac{bm\hbar\omega}{(m\hbar\omega)^2 + b^2} \bar{J}_{n+m}^2 & \text{if} \quad n \geq 1 \end{cases} \tag{4.35}$$

as the shift parameter and

$$\Sigma_n \equiv \frac{\Gamma}{2} \sum_m \frac{b^2}{(m\hbar\omega)^2 + b^2} \bar{J}_{n+m}^2, \tag{4.36}$$

as the width parameter (will be discussed in the next section).

4.3 The Tien-Gordon-like formula

In this section, we derive the Tien-Gordon-like formula for the current using the approximated resultant expression of the GVV perturbation. The memory effect can be described here by two effective parameters (width and shift). The relationship between the peaks of the transmission coefficient and the resultant partial sideband currents are examined numerically.

First, we derive the corresponding approximated eigenstates to obtain the underlying single particle propagator. The evolution propagator $\mathcal{U}(t, t_0)$ for Eq. (4.1) in the initial

unrotated frame may be approximated as

$$\mathcal{U}(t,t_0) \approx \mathcal{R}_n(t)\mathcal{U}^{[n]}_{GVV}(t,t_0)\mathcal{R}_n^{-1}(t_0), \tag{4.37}$$

where $\mathcal{U}^{[n]}_{GVV}(t,t_0)$ is the evolution propagator for Eq. (4.31) in the rotating frame and can be derived explicitly as:

$$\mathcal{U}^{[n]}_{GVV}(t,t_0) = \begin{pmatrix} \mathrm{e}^{-\imath\lambda^{[n]}_+(t-t_0)/\hbar} & 0 \\ 0 & \mathrm{e}^{-\imath\lambda^{[n]}_-(t-t_0)/\hbar} \end{pmatrix}. \tag{4.38}$$

Here, we have only considered the 0-th order terms in Eq. (4.21), i.e.,

$$\begin{cases} |\varphi_{n+}\rangle \approx |\alpha = 1, 0\rangle \\ |\varphi_{n-}\rangle \approx |\alpha = 2, 0\rangle. \end{cases} \tag{4.39}$$

Thus, following Eq. (4.38) and Eq. (4.37,) the single electron propagator propagator in the initial unrotated frame, $U^{[n]}_{GVV}(t,t_0)$, can then be obtained:

$$U(t,t_0) = [\mathcal{U}(t,t_0)]_{11} = \mathrm{e}^{-\imath\frac{A}{\hbar\omega}\sin\omega t}\mathrm{e}^{-\imath\lambda^{[n]}_+(t-t_0)/\hbar}\mathrm{e}^{\imath\frac{A}{\hbar\omega}\sin\omega t_0}. \tag{4.40}$$

In conjunction of Eq. (4.13), leads to the Green's function, cf. Eq. (2.3),

$$G(t,\epsilon) = \sum_{k=-\infty}^{\infty}\sum_{m=-\infty}^{\infty}\frac{J_m(x)J_{m+k}(x)}{\epsilon - \lambda^{[n]}_+ - m\hbar\omega} \times \mathbf{e}^{-\imath k\omega t}, \tag{4.41}$$

and its k-th order Fourier coefficient, cf. Eq. (2.4),

$$G^{(k)}(\epsilon) \approx \sum_{m=-\infty}^{\infty}\frac{J_m(x)J_{m+k}(x)}{\epsilon - \epsilon_0 - m\hbar\omega + \Delta_n + \imath\Sigma_m}. \tag{4.42}$$

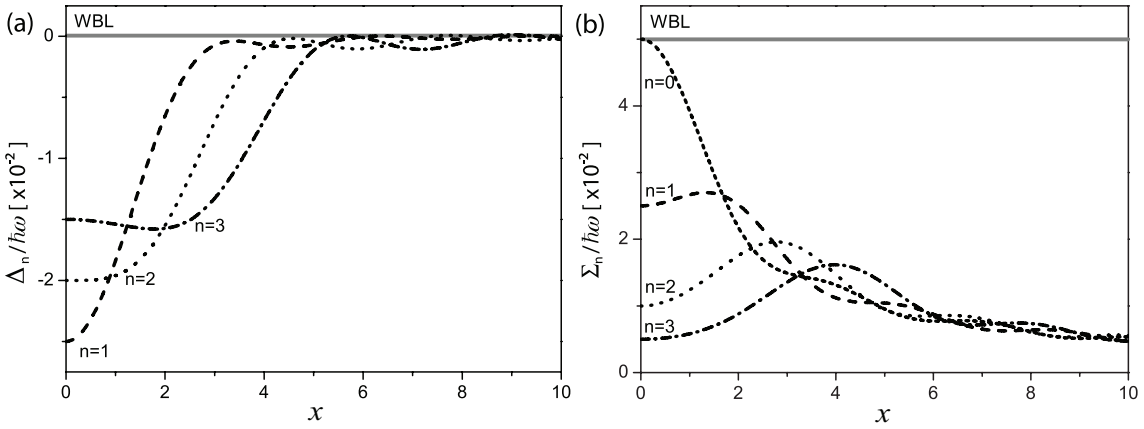

Figure 4.1: The amplitude dependence for (a) the level shift Δ_n and (b) the effective width Σ_n are plotted with respect to various resonance condition, $\epsilon_0 = \sigma - n\hbar\omega$, with $\sigma = 0$. Here, the LSD bandwidth is finite, $b = 1[\hbar\omega]$. The thick gray line indicate the corresponding parameter value in the WBL.

By substituting Eq. (4.42) into Eq. (2.6) and exchanging the summations over m and k, we derive an analytical expression for the transmission coefficient, i. e.,

$$T^{[n]}_{GVV}(\epsilon) = \frac{1}{4}\sum_{m=-\infty}^{\infty} J_m^2 \times \frac{\bar{\Gamma}(\epsilon)\gamma_m(\epsilon)}{(\epsilon - \epsilon_0 - m\hbar\omega + \Delta_n)^2 + \Sigma_n^2}, \tag{4.43}$$

where

$$\gamma_m(\epsilon) = \sum_{k=-\infty}^{\infty} \bar{\Gamma}(\epsilon + k\hbar\omega) J^2_{m+k}(x) = \Gamma \sum_{k=-\infty}^{\infty} \frac{b^2}{(\epsilon + k\hbar\omega)^2 + b^2} J^2_{m+k}(x), \tag{4.44}$$

is the tunneling rate of the m-th PAT sideband [2, 4].

Here the shift and width parameter is clarified as the effective shift and width for the n-photon resonance PAT sideband at the condition $\epsilon_0 = \sigma - n\hbar\omega$. At the high frequency ($\omega >> 1$) and small amplitude ($A \to 0$), both Δ_n and Σ_n are dominated by the term $|J_0(A/\hbar\omega)|^2$ associated with $\ell = -n$. In the limit of $A << \hbar\omega$, we derive that $\Delta_n/\hbar\omega = -nb\Gamma/2[(n\hbar\omega)^2 + b^2] \leq 0$ and $\Sigma_n/\Gamma = b^2/2[(n\hbar\omega)^2 + b^2] \geq 0$.

Fig. 4.1 shows (a) the shift parameter Δ_n and (b) the width parameter Σ_n, cf. Eqs.

(4.35) and (4.36), for the $n = 0, 1, 2, 3$-photon resonance PAT sidebands as functions of the field amplitude parameter $x = A/\hbar\omega$. It is found that in general both magnitudes of the shift and width become smaller as A becomes larger. At the high frequencies and small amplitudes, the corresponding shift and width in Fig. 4.1 can be approximated as $\Delta_n/\hbar\omega \approx -0.05 \times n/(n^2+1)$ and $\Sigma_n/\hbar\omega \approx 0.05/(n^2+1)$, respectively, since $J_0(x) \approx 1$ and $J_\ell(x) \approx 0\ \forall \ell \neq 0$ when $x << 1$. On the other hand, at the low frequencies and large amplitudes, the shift and width become oscillate around zero with decreasingly smaller magnitude, and independent of n, since $|J_\ell(x)|^2 \approx (2/\pi x)\cos^2[x - (2\ell+1)\pi/4]$ when $x >> 1$.

The analytic expression of the n-photon resonance GVV transmission coefficient (between the electrodes and the SQD) is a Tien-Gordon-like formula for the n-photon resonance PAT, which reduces to

$$T_{WBL}(\epsilon) = \frac{1}{4}\sum_{m=-\infty}^{\infty} J_m^2(x) \times \frac{\Gamma^2}{(\epsilon - \epsilon_0 - m\hbar\omega)^2 + \frac{\Gamma^2}{4}} \tag{4.45}$$

in the WBL, just as Eq. (5.8). Both the GVV transmission coefficient, Eq. (4.43), and WBL transmission coefficient, Eq. (4.45), are characterized by a sequence of Lorentzian peaks (sidebands) located at $\epsilon = \sigma + (-n+m)\hbar\omega$, $m = 0, \pm 1, \pm 2, \cdots$. The peaks in the GVV transmission coefficient in general exhibit non-vanishing shifts $\Delta_n \neq 0$ and are narrower than their unshifted WBL counterparts, i.e., $\Sigma_n \leq \Gamma/2$, due to the finite memory effect. From Eqs. (4.6) and (4.43), the corresponding n-photon resonance d.c. current may be approximated by the relation

$$\bar{I}_{GVV}^{[n]} = \sum_{m=-\infty}^{\infty} J_m^2(x) \times \bar{I}_{GVV}^{[n,m]}, \tag{4.46}$$

which is composed of an infinite number of weighted contributing partial currents

$$\bar{I}^{[n,m]}_{GVV} = \frac{e}{4h}\int_{-\infty}^{\infty} \frac{\bar{\Gamma}(\epsilon)\gamma_m(\epsilon)}{(\epsilon-\epsilon_0-m\hbar\omega+\Delta_n)^2+\Sigma_n^2} \times [f_R(\epsilon)-f_L(\epsilon)]d\epsilon,\ m=-\infty,\cdots,+\infty. \tag{4.47}$$

At the zero-temperature, the corresponding d.c. current is determined by the sidebands lying within the bias voltage window $[\mu_R, \mu_L]$, i. e.,

$$\bar{I}^{[n,m]}_{GVV} = \frac{e}{4h}\int_{\mu_R}^{\mu_L} \frac{\bar{\Gamma}(\epsilon)\gamma_m(\epsilon)}{(\epsilon-\epsilon_0-m\hbar\omega+\Delta_n)^2+\Sigma_n^2} d\epsilon,\ m=-\infty,\cdots,+\infty, \tag{4.48}$$

which can be further reduced to

$$\begin{aligned} \bar{I}^{[m]}_{WBL} &= \frac{e}{4h}\Gamma^2\int_{\mu_R}^{\mu_L} \frac{1}{(\epsilon-\epsilon_0-m\hbar\omega)^2+(\Gamma/2)^2} d\epsilon \\ &= \frac{e}{2h}\Gamma\left\{\tan^{-1}\frac{\mu_L-\epsilon_0-m\hbar\omega}{\Gamma/2} - \tan^{-1}\frac{\mu_R-\epsilon_0-m\hbar\omega}{\Gamma/2}\right\}, \end{aligned} \tag{4.49}$$

for $m=-\infty,\cdots,+\infty$, in the WBL, i.e. $b\to\infty$. It is reasonable that Eq. (4.49) is independent of n, since the spectral density is a energy- independent constant that the resonance is invalid for the WBL.

Figure 4.2 depicts the $n=0,1,2$-photon resonance PAT peak pattern of the transmission coefficient $T(\epsilon)$ as a function the spectral energy ϵ at the first root of the zeroth order Bessel function of the first kind $J_0(x)$ where $x=2.406$, showing very good agreement of the GVV results, Eqs. (4.43), and the numerically converged results, Eq. (3.16), see the left panels. It is found that each n-photon resonance PAT transmission coefficient is composed of a sequence of peaks at $\epsilon/\hbar\omega=-n\pm m, m=0,\pm1,\pm2,\cdots$, each approximately

with an amplitude [cf., Eq. (4.43)] equal to

$$\gamma(n,m) \times \frac{\Gamma^2}{4(\Delta_n^2+\Sigma_n^2)} \times \frac{\bar{J}_m^2}{(-n+m)^2+1}, \tag{4.50}$$

where

$$\gamma(n,m) \equiv \sum_{k=-\infty}^{\infty} \frac{\bar{J}_{m+k}^2}{(-n+m+k)^2+1}. \tag{4.51}$$

The PAT peaks at $m=0$ (i.e., $\epsilon/\hbar\omega=-n$) vanish at the roots of $J_0(x)$ (here $x=2.406$ corresponds to the first root), which is a manifestation of the CDT (coherent destruction of tunneling) phenomena [28]. Moreover, the peak patterns of the 1- and 2-photon PAT (and the higher-order ones) are generally not symmetric with respect to the vanished one at $m=0$, due to the asymmetric weights of $\gamma(n,|m|)$ and $\gamma(n,-|m|)$ with respect to the sign change of the peak index m. In the WBL, the corresponding transmission coefficient peak patterns (right panels) are symmetric with respect to one with the zero amplitude at $m=0$, cf. Eq. (4.45) and the peak width Σ_n achieves its maximum value $\Gamma/2$. The insets in the left panels (b) and (c) for the 1- and 2-photon resonances, respectively, show how the position of the peaks near $\epsilon=0$ is shifted, due to the finite spectral density width (here $b=1\hbar\omega << \infty$), at different n-photon resonances in the presence of a periodically driving field.

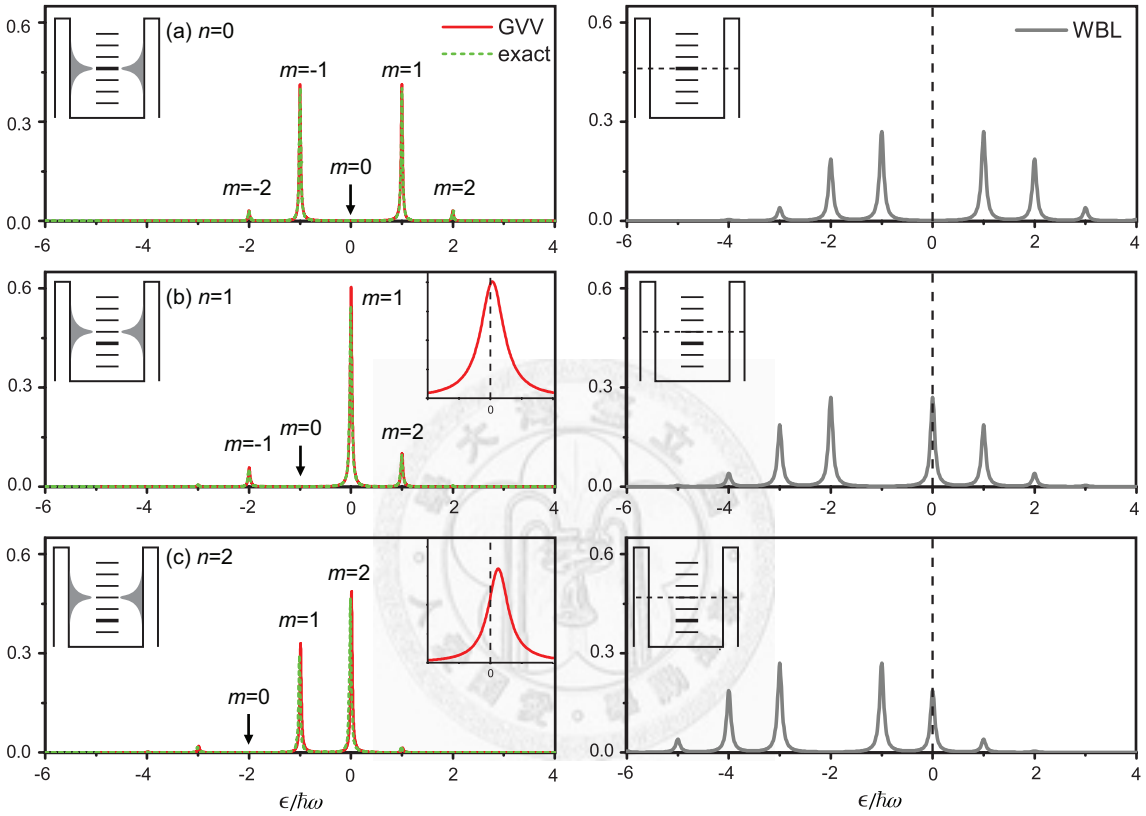

Figure 4.2: Transmission coefficient profiles are shown as a function of the incident energy for the narrow band width case ($b = 1$ $[\hbar\omega]$) in the left panels and for the WBL case in the right panels. The amplitude is chosen as the root of 0-th Bessel function, $x = 2.406$, then we can observe CDT at $m = 0$ sideband. In the left panels, the exact Floquet calculation result (green dot lines) and the analytical GVV result (red solid lines) are compared for the resonance conditions : (a). $n = 0$, (b). $n = 1$, (c). $n = 2$. The insets inside the panel (b) and (c) indicates the peak shift at $\epsilon = 0$. Right panels are corresponding to left panel where the transmission coefficient profiles are merely shift with respect to the reference (the dash line) and symmetric with respect to $m = 0$.

Chapter 5

Temperature-dependence for the wide band limit

5.1 Formulation for symmetric coupling

For simiplicity, we consider the conventional wide band limit (WBL) with symmetric coupling strength (i.e. self-energy in [22]), $\Gamma_L = \Gamma_R = \Gamma/2$. In the WBL, the memory kernel turns out a delta function and,

$$\imath\hbar\frac{\partial}{\partial t}U(t,t_0) = (\epsilon_d + A\cos\omega t)U(t,t_0) - \imath\frac{\Gamma}{2}U(t,t_0), \tag{5.1}$$

can be solved analytically by the formal solution:

$$\psi(t) = \mathrm{e}^{-\imath(\epsilon_0 - \imath\frac{\Gamma}{2})t/\hbar} \times \sum_n J_n(x)e^{-\imath n\omega t} \tag{5.2}$$

where $x = A/\hbar\omega$ and $J_n(x)$ is the n-th order Bessel function of first kind. We have used the well-known expansion, $\mathrm{e}^{\imath x \sin\omega t} = \sum_n J_n(x)\mathrm{e}^{\imath n\omega t}$. The single particle propagator can be written in terms of Bessel functions and casted as

$$U(t, t-\tau) = \sum_{n=-\infty}^{\infty} \left(\sum_{k=-\infty}^{\infty} J_n(x) J_{n+k}(x) \mathrm{e}^{-\imath k\omega t} \right) \times \mathrm{e}^{-\imath(\epsilon_0 + n\hbar\omega - \imath\Gamma)\tau/\hbar}. \tag{5.3}$$

Thus, by inserting this expression into Eq. (2.3) and (2.4), the Fourier component of the retarded Green's function can be written as, explicitly,

$$G^(k)(\epsilon) = \sum_n \frac{J_n(x) J_{n+k}(x)}{\epsilon - \epsilon_0 - n\hbar\omega + \imath\frac{\Gamma}{2}} \tag{5.4}$$

and the transmission coefficient are also symmetric, i.e.

$$T^{(k)}_{LR}(\epsilon) = T^{(k)}_{RL}(\epsilon) = T^{(k)}_{WBL}(\epsilon) = \frac{1}{4}\Gamma^2 |G^{(k)}(\epsilon)|^2. \tag{5.5}$$

We used the addition theorem of the Bessel function

$$J_\nu(u \pm v) = \sum_{k=-\infty}^{\infty} J_{\nu\mp k}(u) J_k(v), \tag{5.6}$$

which carry out the k summation and turn out the delta function in n and n'

$$\sum_{k=-\infty}^{\infty} J_{n+k}(x) J_{n'+k}(x) = J_{n-n'}(0) = \delta_{n,n'}. \tag{5.7}$$

The total transmission coefficient are composed of a collection of peaks located at $\epsilon_0 + n\hbar\omega$,

$$T_{WBL}(\epsilon) = \frac{1}{4}\Gamma^2 \sum_{n=-\infty}^{\infty} \frac{J_n^2(x)}{(\epsilon - \epsilon_0 - n\hbar\omega)^2 + \frac{\Gamma^2}{4}}, \tag{5.8}$$

which can be interpreted as the photon-assisted sidebands generated by the external field. Each sideband possess equivalent width ($\Gamma/2$), but the contribution of each sidebands are weighted by square of the Bessel function of first kind as a function of the amplitude of external field, $J_n^2(x)$. According to the property of the Bessel function, the strong the external field apply, the higher order photon-assisted sideband (larger n) can be accessed.

Explicitly, the d.c. current be written as

$$\bar{I}_{WBL} = \frac{e}{h}\frac{\Gamma^2}{4}\sum_{n=-\infty}^{\infty}\int \frac{J_n^2(x)}{(\epsilon-\epsilon_0-n\hbar\omega)^2+\frac{\Gamma^2}{4}}\{f_R(\epsilon)-f_L(\epsilon)\}d\epsilon. \tag{5.9}$$

and the conductance can be obtained by the derivative of the d.c. current with respect to the bias voltage, $e\mathbf{V} = \mu_L - \mu_R$,

$$\begin{aligned} G &= \frac{d\bar{I}_{WBL}}{d\mathbf{V}} \\ &= \frac{e^2}{h}\frac{\Gamma^2}{4}\sum_{n=-\infty}^{\infty}\int \frac{J_n^2(x)}{(\epsilon-\epsilon_0-n\hbar\omega)^2+\frac{\Gamma^2}{4}}\{\frac{\partial f_R}{\partial \mathbf{V}}(\epsilon)-\frac{\partial f_L}{\partial \mathbf{V}}(\epsilon)\}d\epsilon. \end{aligned} \tag{5.10}$$

We assume the on-site energy $\epsilon_0 = 0$ and $\mu_L = -\mu_R = e\mathbf{V}/2$. The temperature-dependence of the conductance is shown in the Fig. 5.1. At low temperature, $k_B\mathcal{T} \ll \frac{\Gamma}{2}$, each conductance resonance correspond to the contribution of a single sideband for multi-photon process. As the bias voltage increase, one more sideband that participates electron transmission results in one more conductance resonance. However, for the temperatures comparable to the width of sideband $k_B\mathcal{T} \sim \frac{\Gamma}{2}$, the temperature-dependence becomes essential.

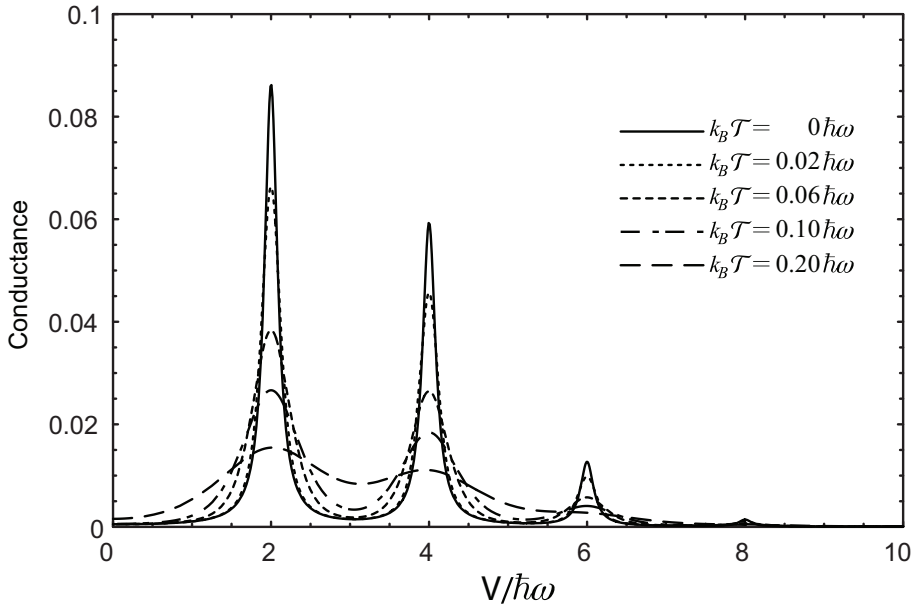

Figure 5.1: Conductance vs the bias voltage for zero temperature (solid line) compared with those for different temperatures:$k_B\mathcal{T} = 0.02, 0.06, 0.1, 0.2\hbar\omega$. We set the external amplitude as $A/\hbar\omega = 2.406$ and the coupling strength $\Gamma_L = \Gamma_R = 0.05\hbar\omega$. The chemical potentials are assumed as $\mu_L = -\mu_R$.

5.2 The zero temperature limit

We just consider the zero temperature limit, $\mathcal{T} = 0$, in which the Fermi-Dirac function turns into a step function. The indefinite integrals are reduced into a definite integration over the bias voltage window, $[\mu_R, \mu_L]$:

$$\begin{aligned}\bar{I}_{[\mathcal{T}=0]} &= \frac{e}{h}\frac{\Gamma^2}{4}\sum_{n=-\infty}^{\infty}\int_{\mu_R}^{\mu_L}\frac{J_n^2(x)}{(\epsilon-\epsilon_0-n\hbar\omega)^2+\frac{\Gamma^2}{4}}d\epsilon \\ &= \frac{e\Gamma}{2h}\sum_{n=-\infty}^{\infty}J_n^2(x)\left(\tan^{-1}(\frac{\mu_L-\epsilon_0-n\hbar\omega}{\Gamma/2})-\tan^{-1}(\frac{\mu_R-\epsilon_0-n\hbar\omega}{\Gamma/2})\right).\end{aligned} \tag{5.11}$$

and the conductance is

$$G_{[\mathcal{T}=0]} = \frac{e^2}{h}\frac{\Gamma^2}{4}\sum_{n=-\infty}^{\infty}J_n^2(x)\left(\frac{d\mu_L/d\mathbf{V}}{(\mu_L-\epsilon_0-n\hbar\omega)^2+\frac{\Gamma^2}{4}}-\frac{d\mu_R/d\mathbf{V}}{(\mu_R-\epsilon_0-n\hbar\omega)^2+\frac{\Gamma^2}{4}}\right). \tag{5.12}$$

For the limit case, we consider $\mu_R \to \infty$ and $\mu_L \to -\infty$ and use the addition theorem

of Bessel fuctions, $\sum_n J_n^2(x) = 1$. Thus, the extreme bias current are denoted by

$$\bar{I}_\infty = \frac{e\pi\Gamma}{2h} \tag{5.13}$$

which depends only on the coupling strength Γ.

5.3 Low temperature limit

In general finite temperature case, $\mathcal{T} \neq 0$, the Fermi-Dirac integration must be carry out by analytical approximation. We can recast the integration by,

$$\int \frac{f_\ell(\epsilon)}{(\epsilon - \epsilon_0 - n\hbar\omega)^2 + \frac{\Gamma^2}{4}} d\epsilon = \int \frac{f_\ell(\epsilon + \epsilon_0 + n\hbar\omega)}{\epsilon^2 + \frac{\Gamma^2}{4}} d\epsilon \tag{5.14}$$

where the Fermi-Dirac function can be expressed by

$$f_\ell(\epsilon + \epsilon_0 + n\hbar\omega) = \frac{1}{1 + z_{\ell,n}(\epsilon)}, \tag{5.15}$$

with $z_{\ell,n}(\epsilon) = \mathrm{e}^{(\epsilon+\epsilon_0+n\hbar\omega-\mu_\ell)/k_B\mathcal{T}}$. Since we treat the zero-temperature limit as the unperturbed case, the parameter turns out, for $\mathcal{T} \to 0$,

$$z_{\ell,n} \to \begin{cases} \infty & \text{if } \epsilon > \mu_\ell - \epsilon_0 - n\hbar\omega \\ 0 & \text{if } \epsilon < \mu_\ell - \epsilon_0 - n\hbar\omega \end{cases} \tag{5.16}$$

Thus, the Fermi-Dirac integration must be approximated in two distinct regions with respect to the following expansions:

1. for $\epsilon > \mu_\ell - \epsilon_0 - n\hbar\omega$ The Fermi-Dirac function are expanded as

$$\frac{1}{1+z_{\ell,n}(\epsilon)} = -\sum_{m=1}^{\infty}(-1)^m \frac{1}{z_{\ell,n}^m(\epsilon)} = \frac{1}{z_{\ell,n}(\epsilon)} - \frac{1}{z_{\ell,n}(\epsilon)^2} + \frac{1}{z_{\ell,n}(\epsilon)^3} + ... \quad (5.17)$$

and the upper part integration turns out

$$\int_{\mu_\ell-\epsilon_0-n\hbar\omega}^{\infty} \frac{f_\ell(\epsilon+\epsilon_0+n\hbar\omega)}{\epsilon^2+\frac{\Gamma^2}{4}} d\epsilon = -\sum_{m=1}^{\infty}\int_0^{\infty} \frac{(-1)^m \mathrm{e}^{-m\epsilon/k_B\mathcal{T}}}{(\epsilon-\epsilon_0-n\hbar\omega+\mu_\ell)^2+\frac{\Gamma^2}{4}} d\epsilon \quad (5.18)$$

2. for $\epsilon < \mu_\ell - \epsilon_0 - n\hbar\omega$ The Fermi-Dirac function are expanded as

$$\frac{1}{1+z_{\ell,n}(\epsilon)} = \sum_{m=0}^{\infty}(-1)^m z_{\ell,n}^m(\epsilon) = 1 - z_{\ell,n}(\epsilon) + z_{\ell,n}(\epsilon)^2 - ... \quad (5.19)$$

and the lower part integration turns out

$$\int_{-\infty}^{\mu_\ell-\epsilon_0-n\hbar\omega} \frac{f_\ell(\epsilon+\epsilon_0+n\hbar\omega)}{\epsilon^2+\frac{\Gamma^2}{4}} d\epsilon = \sum_{m=0}^{\infty}\int_{-\infty}^{0} \frac{(-1)^m \mathrm{e}^{m\epsilon/k_B\mathcal{T}}}{(\epsilon-\epsilon_0-n\hbar\omega+\mu_\ell)^2+\frac{\Gamma^2}{4}} d\epsilon \quad (5.20)$$

Here, the term with $m = 0$ gives the zero-temperature limit (the unperturbed term),

$$\int_{-\infty}^{0} \frac{1}{(\epsilon-\epsilon_0-n\hbar\omega+\mu_\ell)^2+\frac{\Gamma^2}{4}} d\epsilon = \int_{-\infty}^{\mu_\ell} \frac{1}{(\epsilon-\epsilon_0-n\hbar\omega)^2+\frac{\Gamma^2}{4}} d\epsilon \quad (5.21)$$

Therefore, the temperature-dependence of the d.c. current are obtained by combining two parts (lower and upper) and two sides ($\ell = L, R$) and are expressed as

$$\bar{I}_{WBL} = \bar{I}_{[\mathcal{T}=0]} + \sum_{m=1}^{\infty} \bar{I}_{[m]} \quad (5.22)$$

where $\bar{I}_{[\mathcal{T}=0]}$ comes from the combination $m = 0$ terms of two sides, which is corresponding to Eq. (5.11) and $\bar{I}_{[m]}$ are the low-temperature perturbation modification given by

$$\bar{I}_{[m]} = (-1)^m \frac{e}{h}\frac{\Gamma^2}{4}\sum_{n=-\infty}^{\infty} J_n^2(x)\times$$
$$\Bigg(-\int_0^{\infty} \frac{\mathrm{e}^{-m\epsilon/k_B\mathcal{T}}}{(\epsilon-\epsilon_0-n\hbar\omega+\mu_R)^2+\frac{\Gamma^2}{4}}d\epsilon + \int_{-\infty}^{0} \frac{\mathrm{e}^{m\epsilon/k_B\mathcal{T}}}{(\epsilon-\epsilon_0-n\hbar\omega+\mu_R)^2+\frac{\Gamma^2}{4}}d\epsilon$$
$$\int_0^{\infty} \frac{\mathrm{e}^{-m\epsilon/k_B\mathcal{T}}}{(\epsilon-\epsilon_0-n\hbar\omega+\mu_L)^2+\frac{\Gamma^2}{4}}d\epsilon - \int_{-\infty}^{0} \frac{\mathrm{e}^{m\epsilon/k_B\mathcal{T}}}{(\epsilon-\epsilon_0-n\hbar\omega+\mu_L)^2+\frac{\Gamma^2}{4}}d\epsilon \Bigg) \tag{5.23}$$

In the Fig. 5.2, the first order perturbation current $\bar{I}_{[m=1]}$ are compared with exact numerical calculation of the current difference, $\bar{I}_{WBL} - \bar{I}_{[\mathcal{T}=0]}$. For low temperature, the first order perturbation current can describe the temperature dependence of current for the wide band limit. Since the photon energy is approximately $\hbar\omega = 10\ eV$ and $k_B\mathcal{T} \approx 2.5\times10^{-2}\ eV = 0.025\hbar\omega$ at room temperature. Thus, when we assume weak coupling, the current is not very sensitive to the temperature.

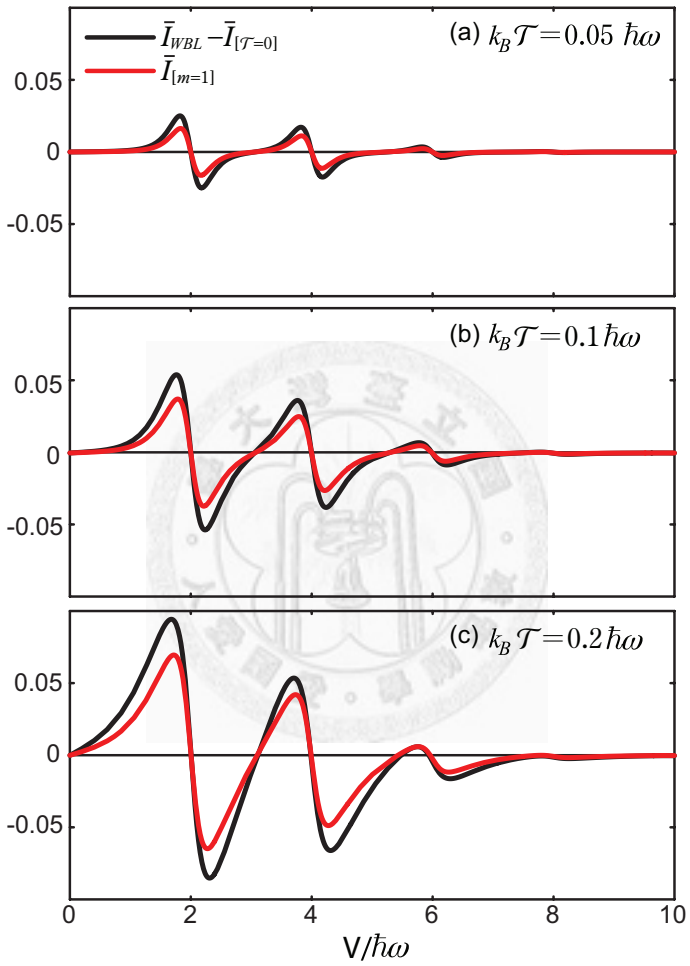

Figure 5.2: The first order ($m = 1$) current perturbation are plotted as a function of voltage window $(\mu_L - \mu_R)/\hbar\omega$ for low temperatures: (a) $\mathcal{T} = 0.05\hbar\omega$, (b) $\mathcal{T} = 0.1\hbar\omega$, and (c) $\mathcal{T} = 0.2\hbar\omega$ and compared with exact numerical calculation by Eq. (5.10) and (5.11). The on-site energy is $\epsilon_0 = 0$ and the external field is $x = A/\hbar\omega = 2.405$.

Chapter 6

Conclusion

In summary, we have developed a generalized Floquet approach, including the memory effect, for the comprehensive treatment of time-dependent electron transport process on a periodically-driven single quantum dot system. The generalized Floquet approach provides an efficient treatment and an insightful picture. We have considered the symmetric single function Lorentzian spectral density model for the electrodes and derived analytical expressions for the transmission coefficient and the d.c. current for the multi-photon resonance PAT phenomena using the generalized Van Vleck theory. By means of the GVV method, the Tien-Gordon PAT formula has been extended to include the memory effect and the multi-photon resonance processes, in particular, resulting in an effective weak-interaction multi-level model of a single quantum dot (one single level with multiple sidebands). The memory effect on the transmission coefficient and the d.c. current has been analyzed at the nearly-degenerate resonance conditions for different external field amplitudes and been described by the effective width and shift of PAT sideband peaks.

Numerical simulations of the transmission coefficient have shown that higher order

multi-photon PAT processes can be suppressed by the memory effect, and the (MP-)CDT phenomena can be predicted by the behavior of transmission coefficient, but not influenced by the memory effect a lot. We have also observe that the stair step feature of the d.c. current is closely related to the PAT peaks in the transmission coefficient. Furthermore, It has been observed that the electron tunneling may be blocked not only if the SQD gate voltage is near the PAT sidebands, but also if the SQD gate voltage is moved outside the narrow band width of the electrode spectral density function. It also imply that the pumped current oscillation may be induced and manipulated by applying periodic external fields, thus, enabling the enhancement or suppression of the d.c. current at certain gate voltages. In addition, we study the temperature-dependence of the conductance for the wide band limit, showing temperature affect only if comparable to the coupling strength. An analytical expression of of the temperature-dependence of the d.c. current by perturbation method.

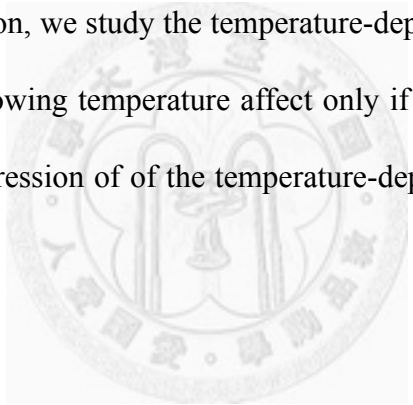

Bibliography

[1] A. H. Dayem and R. J. Martin. Quantum interaction of microwave radiation with tunneling between superconductors. *Phys. Rev. Lett.*, 8(6):246–248, Mar 1962.

[2] P. K. Tien and J. P. Gordon. Multiphoton process observed in the interaction of microwave fields with the tunneling between superconductor films. *Phys. Rev.*, 129(2):647–651, Jan 1963.

[3] L. P. Kouwenhoven, S. Jauhar, J. Orenstein, P. L. McEuen, Y. Nagamune, J. Motohisa, and H. Sakaki. Observation of photon-assisted tunneling through a quantum dot. *Phys. Rev. Lett.*, 73(25):3443–3446, Dec 1994.

[4] L. P. Kouwenhoven, S. Jauhar, K. McCormick, D. Dixon, P. L. McEuen, Yu. V. Nazarov, N. C. van der Vaart, and C. T. Foxon. Photon-assisted tunneling through a quantum dot. *Phys. Rev. B*, 50(3):2019–2022, Jul 1994.

[5] T. Fujisawa and S. Tarucha. Photon assisted tunneling in single and coupled quantum dot system. *Superlattices and Microstructures*, 21(2), 1997.

[6] T. H. Oosterkamp, L. P. Kouwenhoven, A. E. A. Koolen, N. C. van der Vaart, and C. J. P. M. Harmans. Photon sidebands of the ground state and first excited state of a quantum dot. *Phys. Rev. Lett.*, 78(8):1536–1539, Feb 1997.

[7] Enrico Prati, Rossella Latempa, and Marco Fanciulli. Microwave-assisted transport in a single-donor silicon quantum dot. *Phys. Rev. B*, 80(16):165331, Oct 2009.

[8] Rossella Latempa Enrico Prati and Marco Fanciulli. *Electron Spin Resonance and Related Phenomena in Low-Dimensional Structures*, volume 115 of *Topics in Applied Physics*, pages 241–258. Springer Berlin / Heidelberg, 2009.

[9] Kouwenhoven LP Meyer C, Elzerman JM. Photon-assisted tunneling in a carbon nanotube quantum dot. *Nano Letter*, 7(2):295–299, 2007.

[10] T H Oosterkamp, L P Kouwenhoven, A E A Koolen, N C van der Vaart, and C J P M Harmans. Photon-assisted tunnelling through a quantum dot. *Semicond. Sci. Technol.*, 11:1512–1515, 1996.

[11] C. Bruder and H. Schoeller. Charging effects in ultrasmall quantum dots in the presence of time-varing fields. *Phys. Rev. Lett.*, 72(7):1076–1079, Feb 1994.

[12] Antti-Pekka Jauho, Ned S. Wingreen, and Yigal Meir. Time-dependent transport in interacting and noninteracting resonant-tunneling systems. *Phys. Rev. B*, 50(8):5528–5544, Aug 1994.

[13] Ned S. Wingreen, Antti-Pekka Jauho, and Yigal Meir. Time-dependent transport through a mesoscopic structure. *Phys. Rev. B*, 48(11):8487–8490, Sep 1993.

[14] Gloria Platero and Ramon Aguado. Photon-assisted transport in semiconductor nanostructures. *Physics Reports*, 395:1–157, 2004.

[15] Ramón Aguado, Jesús Iñarrea, and Gloria Platero. Coherent resonant tunneling in ac fields. *Phys. Rev. B*, 53(15):10030–10041, Apr 1996.

[16] Yigal Meir, Ned S. Wingreen, and Patrick A. Lee. Transport through a strongly interacting electron system: Theory of periodic conductance oscillations. *Phys. Rev. Lett.*, 66(23):3048–3051, Jun 1991.

[17] A.A.M. Staring H. van Houten, C.W.J. Beenakker. Coulomb-blockade oscillations in semiconductor nanostructures. *arXiv:cond-mat*, (0508454v1), 2005.

[18] Qing-feng Sun and Tsung-han Lin. Influence of microwave fields on the electron tunneling through a quantum dot. *Phys. Rev. B*, 56(7):3591–3594, Aug 1997.

[19] Qing-feng Sun, Jian Wang, and Tsung-han Lin. Photon sidebands of the ground state and the excited state of a quantum dot: A nonequilibrium green-function approach. *Phys. Rev. B*, 58(19):13007–13014, Nov 1998.

[20] Qing-feng Sun, Jian Wang, and Tsung-han Lin. Theory of excess noise of a quantum dot in the presence of a microwave field. *Phys. Rev. B*, 61(19):13032–13036, May 2000.

[21] T. Kwapiński, R. Taranko, and E. Taranko. Band structure effects in time-dependent electron transport through the quantum dot. *Phys. Rev. B*, 66(3):035315, Jul 2002.

[22] Sigmund Kohler, Jorg Lehmann, and Peter Hanggi. Driven quantum transport on the nanoscale. *Phys. Rep.*, 406(6):379–443, 2005.

[23] Sébastien Camalet, Sigmund Kohler, and Peter Hänggi. Shot-noise control in ac-driven nanoscale conductors. *Phys. Rev. B*, 70(15):155326, Oct 2004.

[24] Sven Welack, Michael Schreiber, and Ulrich Kleinekathofer. The influence of ultra-fast laser pulses on electron transfer in molecular wires studied by a non-markovian density-matrix approach. *The Journal of Chemical Physics*, 124(4):044712, 2006.

[25] Coherent control of the spin current through a quantum dot. *The European Physical Journal B*, 2009.

[26] Time-dependent suppression of current through molecular junctions. *physica status solidi (b)*, page NA, 2008.

[27] GuangQi Li, Michael Schreiber, and Ulrich Kleinekathöfer. Suppressing the current through molecular wires: comparison of two mechanisms. *New Journal of Physics*, 10(8):085005, 2008.

[28] G.-Q. Li, M. Schreiber, and U. Kleinekathofer. Coherent laser control of the current through molecular junctions. *Europhysics Letters*, 79(2):27006, 2007.

[29] Brahim Elattari and S. A. Gurvitz. Influence of measurement on the lifetime and the linewidth of unstable systems. *Phys. Rev. A*, 62(3):032102, Aug 2000.

[30] Matisse W. Y. Tu and Wei-Min Zhang. Non-markovian decoherence theory for a double-dot charge qubit. *Phys. Rev. B*, 78(23):235311, Dec 2008.

[31] Philipp Zedler, Gernot Schaller, Gerold Kiesslich, Clive Emary, and Tobias Brandes. Weak-coupling approximations in non-markovian transport. *Phys. Rev. B*, 80(4):045309, Jul 2009.

[32] Tak-San Ho, Shih-Han Hung, Hsing-Ta Chen, and Shih-I Chu. Memory effect on the multiphoton coherent destruction of tunneling in the electron transport of nanoscale systems driven by a periodic field: A generalized floquet approach. *Phys. Rev. B*, 79(23):235323, Jun 2009.

[33] Jon H. Shirley. Solution of the schrödinger equation with a hamiltonian periodic in time. *Phys. Rev.*, 138(4B):B979–B987, May 1965.

[34] Gaston Floquet. Sur les équations différentielles linéaires à coefficients périodiques. *Ann. École Norm. Sup.*, 12(47–88), 1883.

[35] Shih-I Chu. Recent developments in semiclassical Floquet theories for intense-field multiphoton processes. In *Advances in Atomic and Molecular Physics*, volume 21, pages 197–253. Academic Press, New York, 1985.

[36] Shih-I Chu. Generalized Floquet theoretical approaches to multiphoton and non-linear optical processes in intense laser fields. In *Advances in Chemical Physics*, volume 73, pages 739–799. John Wiley & Sons, New York, 1989.

[37] Shih-I Chu and Dmitry A. Telnov. Beyond the floquet theorem: generalized floquet formalisms and quasienergy methods for atomic and molecular multiphoton processes in intense laser fields. *Phys. Rep.*, 390:1–131, 2004.

[38] Shih-I Chu and William P. Reinhardt. Intense field multiphoton ionization via complex dressed states: Application to the h atom. *Phys. Rev. Lett.*, 39(19):1195–1198, Nov 1977.

[39] Shih-I Chu and J. Cooper. Threshold shift and above-threshold multiphoton ionization of atomic hydrogen in intense laser fields. *Phys. Rev. A*, 32(5):2769–2775, Nov 1985.

[40] J. Y. Wang, S. I. Chu, and C. Laughlin. Multiphoton detachment of H^-. II. Intensity-dependent photodetachment rates and threshold behavior – complex-scaling generalized pseudospectral method. *Phys. Rev. A*, 50(4):3208–3215, 1994.

[41] D. A. Telnov and S. I. Chu. Electron angular distributions after above-threshold multiphoton detachment of H^- by 1064 nm radiation. *J. Phys. B: At. Mol. Opt. Phys.*, 29:4401–4410, 1996.

[42] Shih-I Chu. Floquet theory and complex quasivibrational energy formalism for intense field molecular photodissociation. *The Journal of Chemical Physics*, 75(5):2215–2221, 1981.

[43] G. H. Yao and S. I. Chu. Laser-induced molecular stabilization and trapping and chemical bond hardening in intense laser fields. *Chem. Phys. Lett.*, 197(4-5):413–418, 1992.

[44] X. Chu and S. I. Chu. Complex-scaling generalized pseudospectral method for quasienergy resonance states in two-center systems: Application to the Floquet study of charge resonance enhanced multiphoton ionization of molecular ions in intense low-frequency laser fields. *Phys. Rev. A*, 63(1):013414, 2000.

[45] D. A. Telnov and S. I. Chu. Effects of electron structure and multielectron dynamical response on strong-field multiphoton ionization of diatomic molecules with arbitrary orientation: An all-electron time-dependent density-functional-theory approach. *Phys. Rev. A*, 79:041401(R), 2009.

[46] Tak-San Ho, Shih-I Chu, and J. V. Tietz. Semiclassical many-mode Floquet theory. *Chem. Phys. Lett.*, 96:464–471, 1983.

[47] T. S. Ho and S. I. Chu. Semiclassical many-mode Floquet theory. II. Non-linear multiphoton dynamics of a 2-level system in a strong bichromatic field. *J. Phys. B: At. Mol. Phys.*, 17:2101–2128, 1984.

[48] T. S. Ho and S. I. Chu. Semiclassical many-mode Floquet theory. III. SU(3) dynamical evolution of three-level systems in intense bichromatic fields. *Phys. Rev. A*, 31:659–676, 1985.

[49] Dmitry A. Telnov, Jingyan Wang, and Shih-I Chu. Above-threshold multiphoton detachment of $h-$ by two-color laser fields: Angular distributions and partial rates. *Phys. Rev. A*, 51(6):4797–4808, Jun 1995.

[50] Dmitry A. Telnov, Jingyan Wang, and Shih-I Chu. Two-color phase control of high-order harmonic generation in intense laser fields. *Phys. Rev. A*, 52(5):3988–3996, Nov 1995.

[51] Tak-San Ho and Shih-I Chu. Floquet-Liouville super-matrix approach for multiphoton non-linear optical processes in intense laser fields. *Chem. Phys. Lett.*, 122(4):327–332, 1985.

[52] Tak-San Ho, Kwanghsi Wang, and Shih-I Chu. Floquet-liouville supermatrix approach: Time development of density-matrix operator and multiphoton resonance fluorescence spectra in intense laser fields. *Phys. Rev. A*, 33(3):1798–1816, Mar 1986.

[53] Kwanghsi Wang and Shih-I Chu. Floquet–liouville supermatrix approach. ii. intensity-dependent generalized nonlinear optical susceptibilities. *The Journal of Chemical Physics*, 86(6):3225–3238, 1987.

[54] S. Han, Y. Yu, X. Chu, S. I. Chu, and Z. Wang. Time-resolved measurement of dissipation-induced decoherence in a Josephson junction. *Science*, 293(5534):1457–1459, 2001.

[55] Y. Yu, S. Han, X. Chu, S. I. Chu, and Z. Wang. Coherent temporal oscillations of macroscopic quantum states in a Josephson junction. *Science*, 296(5569):889–892, 2002.

[56] Phillip R. Certain and Joseph O. Hirschfelder. New partitioning perturbation theory. i. general formalism. *The Journal of Chemical Physics*, 52(12):5977–5987, 1970.

[57] Tak-San Ho and Shih-I Chu. Semiclassical many-mode floquet theory. iii. su(3) dynamical evolution of three-level systems in intense bichromatic fields. *Phys. Rev. A*, 31(2):659–676, Feb 1985.

[58] Sang-Kil Son, Siyuan Han, and Shih-I Chu. Floquet formulation for the investigation of multiphoton quantum interference in a superconducting qubit driven by a strong ac field. *Phys. Rev. A*, 79(3):032301, Mar 2009.